PHILOSOPHICAL TRANSACTIONS A

royalsocietypublishing.org/journal/rsta

Research

**Cite this article:** Frohoff-Hülsmann T, Thiele U, Pismen LM. 2023 Non-reciprocity induces resonances in a two-field Cahn–Hilliard model. *Phil. Trans. R. Soc. A* **381**: 20220087. https://doi.org/10.1098/rsta.2022.0087

Received: 29 September 2022
Accepted: 9 January 2023

One contribution of 18 to a theme issue 'New trends in pattern formation and nonlinear dynamics of extended systems'.

**Subject Areas:**
complexity, mathematical modelling

**Keywords:**
active matter, pattern formation, weakly nonlinear analysis, non-reciprocal Cahn–Hilliard model, conserved FitzHugh–Nagumo model, Hopf–Turing resonance

**Authors for correspondence:**
Tobias Frohoff-Hülsmann
e-mail: t_froh01@uni-muenster.de
Uwe Thiele
e-mail: u.thiele@uni-muenster.de



# Non-reciprocity induces resonances in a two-field Cahn–Hilliard model

Tobias Frohoff-Hülsmann[1], Uwe Thiele[1,2] and Len M. Pismen[3]

[1]Institut für Theoretische Physik, Westfälische Wilhelms-Universität Münster, Wilhelm-Klemm-Str. 9, Münster 48149, Germany
[2]Center for Nonlinear Science (CeNoS), Westfälische Wilhelms-Universität Münster, Corrensstr. 2, Münster 48149, Germany
[3]Department of Chemical Engineering, Technion—Israel Institute of Technology, Haifa 32000, Israel

TF-H, 0000-0002-5589-9397; UT, 0000-0001-7989-9271; LMP, 0000-0002-9932-4165

We consider a non-reciprocally coupled two-field Cahn–Hilliard system that has been shown to allow for oscillatory behaviour and suppression of coarsening. After introducing the model, we first review the linear stability of steady uniform states and show that all instability thresholds are identical to the ones for a corresponding two-species reaction–diffusion system. Next, we consider a specific interaction of linear modes—a 'Hopf–Turing' resonance—and derive the corresponding amplitude equations using a weakly nonlinear approach. We discuss the weakly nonlinear results and finally compare them with fully nonlinear simulations for a specific conserved amended FitzHugh–Nagumo system. We conclude with a discussion of the limitations of the employed weakly nonlinear approach.

This article is part of the theme issue 'New trends in pattern formation and nonlinear dynamics of extended systems'.

## 1. Introduction

Breaking Newton's third law has recently become a cherished pastime for theoretical physicists and applied mathematicians alike [1–5]. This not only formally breaks the boring symmetry in particle–particle interactions,



THE ROYAL SOCIETY PUBLISHING

but has dire consequences for the system's behaviour: particles are not anymore attracted or repelled by their common centre of mass (that remains at rest) but instead may start a chasing race as one (the 'predator') is attracted by the other one, while the latter (the 'prey') is repelled by the first one [6].

In this way, oscillations and persistent motion may not only emerge for particle-based models but also characterize collective behaviour as described by continuum models, e.g. non-reciprocal Cahn–Hilliard (CH) models [5,7,8], thereby providing a 'generic route to traveling states' [5].[1] The non-reciprocal CH model is also particularly relevant because it keeps all conservation laws intact, in contrast to models considered, e.g. in [10]. The importance of conservation laws for pattern formation has been widely discussed: Matthews & Cox [11] and Winterbottom et al. [12] analyse small-scale stationary and oscillatory instabilities in the presence of a conservation law, which are relevant for pattern formation in a wide spectrum of systems, e.g. in magnetoconvection [13], in crystallization of passive and active colloids [14,15] and in the dynamics of the actin cortex of motile cells [16,17]. It has been recently shown that the standard CH model (introduced to describe phase separation in a binary mixture [18,19]) also corresponds to an amplitude equation valid close to a large-scale stationary instability in systems with a single conservation law [20]. This implies that reaction–diffusion (RD) systems with one conservation law, studied, e.g. in [16,21–26], may be described in the vicinity of a large-scale stationary instability by a CH equation. In general, such considerations are highly relevant for the modelling of a large spectrum of biochemophysical systems ranging from proteins or the cytoplasm within biological cells to the dynamics of active colloids, microswimmers, tissues or human (or robotic) crowds [1,2,27–34]. For a more extensive introduction to the non-reciprocal CH model within a wider context, see [7]. Its universal importance is considered in [35].

Bifurcationally speaking, above a critical value of the non-reciprocal coupling mediated by non-equilibrium chemical potentials that keep both conservation laws intact, oscillatory and travelling states emerge via Hopf and drift (pitchfork and transcritical) bifurcations from steady periodic or localized patterns [7,36]. Even though the conservation laws play an important role in the instabilities, this is similar to many other widely studied systems, e.g. RD models [37–40] and active phase-field crystal models [41–43]. Remarkably, the non-reciprocal interactions may also result in the transformation of a stationary large-scale instability (CH instability) typical for phase separation [44] into a stationary small-scale Turing-like instability with mass conservation (conserved-Turing instability). The Turing instability is well known from RD systems without mass conservation [45]. In consequence of such a transformation, in CH models, non-reciprocity may cause complete suppression or arrest of coarsening [7] as well as the emergence of localized states [36] with a slanted homoclinic snaking typical for systems with a conservation law [13,46].

The original one-field passive CH model describes phase separation of binary fluid phases or isotropic solids [18,19]. Eminent examples of non-variational one-field variants include the convective CH model (broken parity symmetry) [47,48] and models extended by non-equilibrium chemical potentials that describe motility-induced phase separation [49,50]. Two-field passive CH models feature a reciprocal coupling between species and are employed, e.g. to study phase separation in ternary mixtures driven by gradients of the corresponding chemical potentials [51–54]. Non-equilibrium conditions are readily attained when two interacting number-conserving species are present. It is sufficient to make their interactions non-reciprocal [7,8]. Particles of one kind may be attracted by particles of another kind, while the latter may be repelled by the former. Relations of this kind naturally occur between predators and prey or between parasitic and cooperating bacteria or between catalytic particles with different phoretic response to chemical(s) produced by particles of another type. The analysis to follow reveals both, parallels and differences between symmetry-breaking bifurcations in active systems with mass conservation and in RD systems with autocatalytic components. A combination of conserved and non-conserved species has been also considered in the framework of arrested

[1]For a discussion of genericity, see [9].

phase separation [55]. Two-field CH models with additional reaction terms in both equations (i.e. with non-variational non-mass-conserving couplings) are also widely studied, e.g. in [10,56,57].

In this communication, we reconsider the non-reciprocally coupled CH model (§2) studied in [7] and discuss it as a fully mass-conserving equivalent to the classical Turing two-species RD system (§3). Then we show that, in consequence, resonances exist between conserved-Hopf instability and conserved-Turing instability, i.e. the conserved equivalents of Hopf and Turing instability, respectively. This occurs in the vicinity of the codimension-two point where these two linear instabilities occur simultaneously (§4). The modified FitzHugh–Nagumo system is considered as a specific example in §5. We close with a conclusion and an outlook in §6.

## 2. Cahn–Hilliard system with non-reciprocal coupling

A non-reciprocal CH model describes interactions between two species with concentrations $u(\mathbf{x},t)$ and $v(\mathbf{x},t)$, where the effective non-equilibrium chemical potential of each species depends asymmetrically on the concentration of the other species:

$$\mu_u = \frac{\delta \mathcal{F}}{\delta u} + \mu_u^{\mathrm{nv}} \quad \text{and} \quad \mu_v = \frac{\delta \mathcal{F}}{\delta v} + \mu_v^{\mathrm{nv}}, \tag{2.1}$$

where

$$\mathcal{F} = \int \mathrm{d}\mathbf{x} \left( \frac{\kappa_u}{2} |\nabla u|^2 + \frac{\kappa_v}{2} |\nabla v|^2 + \chi(u,v) \right) \tag{2.2}$$

is the free energy functional with the general local potential $\chi(u,v)$. The non-variational part of the chemical potentials $\mu_u^{\mathrm{nv}}$ and $\mu_v^{\mathrm{nv}}$ (both assumed to depend on $u$ and $v$) cannot be obtained from a common functional, so that $\partial_v \mu_u^{\mathrm{nv}} \neq \partial_u \mu_v^{\mathrm{nv}}$. Introducing the chemical potentials into the conservation laws $\partial_t u = -\nabla \cdot \mathbf{j}_u$ with $\mathbf{j}_u = -\gamma_u \nabla \mu_u$ (and similar for $v$) leads, after rescaling time and length, to the non-reciprocally coupled CH equations:

$$\frac{\partial}{\partial t} u = -\nabla^2 [\nabla^2 u + f(u,v)] \quad \text{and} \quad \frac{\partial}{\partial t} v = -\nabla^2 [\sigma \nabla^2 v + g(u,v)], \tag{2.3}$$

where $\sigma = \gamma\kappa$ is the product of the ratios of mobilities $\gamma = \gamma_v/\gamma_u$ and rigidities $\kappa = \kappa_v/\kappa_u$ of the two species. Based on the functional (2.2), the local terms in (2.3) are then $f = -(\partial_u \chi + \mu_u^{\mathrm{nv}})$ and $g = -\gamma(\partial_v \chi + \mu_v^{\mathrm{nv}})$.

Note that dropping the outer Laplace operator $-\nabla^2$ from the mass-conserving system (2.3) directly results in a typical two-species RD system, i.e. a system without mass conservation [58]. In the corresponding RD system, the parameter $\sigma$ represents the ratio of diffusion constants, while $f$ and $g$ represent the reaction terms. Below, we use this equivalence to relate the linear stability of uniform steady states of a non-reciprocal CH system directly to the linear stability of such states in RD systems. Due to mass conservation, in the CH system, any homogeneous state $(u,v) = (u_s, v_s)$ automatically corresponds to a steady state. By contrast, for an RD system, this requires adjustments of the constant parts of $f$ and $g$. We consider the linear stability of $(u_s, v_s)$ and show that a non-reciprocal coupling does not only allow for the classical CH instability (i.e. a large-scale stationary instability with a conservation law) but may also result in a conserved-Turing instability (i.e. a small-scale stationary instability with a conservation law) as studied in [11,59] and a conserved-Hopf instability (i.e. a large-scale oscillatory instability with a conservation law). Here, the largest available scale replaces homogeneous oscillations of a standard Hopf instability that are incompatible with conservation laws.

## 3. Linear stability: relation between conserved and non-conserved dynamics

### (a) Classification of instabilities

Before presenting the linear analysis of the model (2.3), we introduce in table 1 our classification of instabilities, for a detailed discussion, see [35]. In the literature, the Cross–Hohenberg classification [60] is often used. However, here, it is not a good choice, because, in our opinion, it

**Table 1.** Naming convention of linear instabilities classified via their temporal (stationary versus oscillatory) and spatial (homogeneous/large-scale versus small-scale) properties for non-conserved and conserved dynamics. For reference, we give in parentheses the existing names of the instabilities in the classification by Cross & Hohenberg [60]. For further explanations, see the main text.

| | non-conserved dynamics | conserved dynamics |
|---|---|---|
| homogeneous/large-scale, stationary | Allen–Cahn ($\mathrm{III}_s$) | Cahn–Hilliard ($\mathrm{II}_s$) |
| homogeneous/large-scale, oscillatory | Hopf[a] ($\mathrm{III}_o$) | conserved-Hopf ($\mathrm{II}_o$) |
| small-scale, stationary | Turing ($\mathrm{I}_s$) | conserved-Turing (–) |
| small-scale, oscillatory | wave[b] ($\mathrm{I}_o$) | conserved-wave (–) |

[a]Also known as 'Poincaré-Andronov-Hopf'.

[b]Sometimes also called 'finite-wavelength Hopf' or 'oscillatory Turing'.

does not clearly distinguish between the conserved dynamics, i.e. the model (2.3), and the non-conserved dynamics, i.e. the corresponding RD system (equation (2.3) without the leading $-\nabla^2$). In table 1, we distinguish two main classes—non-conserved and conserved dynamics—each divided into four subclasses depending on the spatial and temporal character of the growing modes near the onset.

First, if the imaginary part of the temporal eigenvalue is zero, the unstable mode grows monotonically—the instability is stationary, if not, it defines the temporal frequency of the oscillation—the instability is oscillatory. Second, the wavenumber encoding the spatial structure of the unstable mode at onset is either zero or finite. In the former case, one has an homogeneous or large-scale instability, and in the latter case, the wavenumber defines the characteristic length scale of a small-scale instability.[2] In the non-conserved case, the instability at $k=0$ always corresponds to a homogeneous (or global) mode, as each point of a finite or infinite domain grows monotonically or oscillatory without any spatial modulation. Thus, we refer to it as a 'homogeneous instability'. Such an homogeneous behaviour is, however, incompatible with a fully conserved dynamics.[3] Instead, the stationary or oscillatory mode with the smallest wavenumber compatible with the boundary conditions is excited, e.g. for periodic boundary conditions its wavelength equals the domain size. In the oscillatory case, this is called a conserved-Hopf instability. In the following, we address all linear instabilities by the names given in table 1.

## (b) Instability thresholds

Using the ansatz $(u,v)=(u_s,v_s)+\varepsilon(u_1,v_1)\exp(\lambda t+\mathrm{i}\mathbf{k}\cdot\mathbf{x})$ with $\varepsilon\ll 1$, and abbreviating partial derivatives with respect to $u$ and $v$ as subscripts, e.g. $\frac{\partial}{\partial u}f=f_u$, the linearized equations (2.3) are expressed as follows:

$$(\underline{\mathbf{L}}(k^2)-\lambda\underline{\mathbf{1}})\begin{pmatrix}u_1\\v_1\end{pmatrix}=\mathbf{0}\quad\text{with }\underline{\mathbf{L}}(k^2)=k^2\begin{pmatrix}f_u-k^2 & f_v\\ g_u & g_v-\sigma k^2\end{pmatrix}=k^2\widetilde{\underline{\mathbf{L}}}(k^2). \tag{3.1}$$

The derivatives in the Jacobian matrix $\underline{\mathbf{L}}$ are computed at the homogeneous state $(u_s,v_s)$, which we do not need to specify. The eigenvalues are given by

$$\lambda=k^2\tilde{\lambda}\quad\text{with }\tilde{\lambda}=\frac{\mathrm{tr}\,\widetilde{\underline{\mathbf{L}}}}{2}\pm\sqrt{\frac{(\mathrm{tr}\,\widetilde{\underline{\mathbf{L}}})^2}{4}-\det\widetilde{\underline{\mathbf{L}}}}. \tag{3.2}$$

[2]Small-scale and large-scale instability are also referred to as 'short-wave' and 'long-wave' instability, respectively. Alternatively, but much less frequently, also 'short-scale' and 'long-scale' instability are used [61].

[3]This is the case for model (2.3) where all components are conserved. For systems with fewer conserved quantities than dynamically evolving fields, homogeneous oscillations compatible with the conservation law are possible. In such a case, the Hopf mode resulting from at least two non-conserved quantities has to be considered in conjunction with also existing neutral modes due to the conserved quantities.

It is important to note that the expression (3.1) differs from the classical Turing problem of the linear stability of a two-component RD system [45,58] solely by the factor $k^2$. This implies that $\det \underline{\mathbf{L}}(k^2)$ has zeros wherever $\det \underline{\tilde{\mathbf{L}}}(k^2)$ does. Moreover, since thresholds of symmetry-breaking instabilities correspond to zero crossings of maxima of $\mathrm{Re}\lambda(k^2)$ (where its derivative with respect to $k^2$ vanishes), whenever both $\mathrm{Re}\tilde{\lambda}(k^2)=0$ and $\partial_{k^2}[\mathrm{Re}\tilde{\lambda}(k^2)]=0$, also $\mathrm{Re}\lambda(k^2)=0$ and $\partial_{k^2}[\mathrm{Re}\lambda(k^2)]=\partial_{k^2}[k^2\mathrm{Re}\tilde{\lambda}(k^2)]=0$, implying identical instability thresholds in the conserved and non-conserved case.[4] Therefore, the stability diagrams for homogeneous states of model (2.3) and of the corresponding RD model are identical. The discussed equivalence directly implies that the product of the ratios of mobilities and rigidities in the non-reciprocal CH system (conserved case) $\sigma$ takes the role of the ratio of diffusion constants in the corresponding RD system (non-conserved case). However, besides their zero crossings, the dispersion relations in a conserved ($\lambda(k)$) and non-conserved ($\tilde{\lambda}(k)$) case are different, and distinctions between the two cases are important for nonlinear analysis and detection of secondary instabilities.

The instability thresholds for a conserved system can therefore be established by analysing the eigenvalues $\tilde{\lambda}$ for the non-conserved case. The onset of all stationary instabilities, i.e. with $\mathrm{Re}\,\tilde{\lambda}=\mathrm{Im}\,\tilde{\lambda}=0$, is determined by $\det \underline{\tilde{\mathbf{L}}}=0$, i.e.

$$0=f_u g_v - f_v g_u - k^2(\sigma f_u + g_v) + \sigma k^4 \equiv A - k^2 B + \sigma k^4, \tag{3.3}$$

which gives the following wavenumbers of marginally stable modes

$$k_\pm^2 = \frac{B}{2\sigma}\left[1 \pm \sqrt{1-\frac{4\sigma A}{B^2}}\right]. \tag{3.4}$$

Equation (3.4) can have zero, one or two positive real solutions. In the latter two cases, the band of wavenumbers corresponding to positive real eigenvalues is $[0,k_\pm]$ and $[k_-,k_+]$, respectively.[5] If $B<0$ only $k_-$ can be real and only if $A=f_u g_v - f_v g_u<0$. The onset occurs at $k_-=0$ for $A=0$, i.e.

$$f_u = g_v^{-1} f_v g_u. \tag{3.5}$$

This corresponds to an Allen–Cahn instability (table 1). If $B>0$, both $k_+$ and $k_-$ are real if $(B^2/4\sigma)\geq A\geq 0$. A Turing instability occurs if $k_+=k_-$, i.e. with critical wavenumber

$$k_T^2 = k_\pm^2 = \frac{B}{2\sigma} = \frac{\sigma f_u + g_v}{2\sigma} = \frac{g_v \pm \sqrt{-\sigma f_v g_u}}{\sigma}. \tag{3.6}$$

This instability appears at $A=B^2/4\sigma$, i.e. at $\sigma f_u = g_v \pm 2\sqrt{-\sigma f_v g_u}$ if the trace

$$\mathrm{tr}\,\underline{\tilde{\mathbf{L}}} = f_u + g_v - k_T^2(1+\sigma) \tag{3.7}$$

is negative, otherwise it would correspond to a minimum of the dispersion relation instead of a maximum. That is, for an RD system, a Turing instability requires at least one species to be autocatalytic ($B>0$) and, additionally, $(1-\sigma)(\sigma f_u - g_v)<0$, which is proven by inserting $k_T$ (3.6) into the trace (3.7) that has to be negative. Here, we choose $u$ as the only autocatalytic species, i.e. we assume $f_u>0, g_v<0$, so that a Turing instability only occurs[6] if $\sigma>1$ at

$$\sigma f_u = g_v + 2\sqrt{-\sigma f_v g_u} > |g_v|. \tag{3.8}$$

This means that non-reciprocity via $f_v g_u<0$ is another necessary condition, i.e. a reciprocal interaction always prevents a Turing instability. When $A$ crosses zero for $B>0$, $k_-$ becomes again complex, i.e. then $k_+$ is the only remaining root of the dispersion relation. However, this does

[4]The determinant $\det \underline{\mathbf{L}}(k^2)$ has then, in addition to the zeros of $\det \underline{\tilde{\mathbf{L}}}(k^2)$, a persistent zero at $k=0$. This may be irrelevant for linear stability but is important for weakly nonlinear analysis.

[5]Provided that $\mathrm{tr}\underline{\tilde{\mathbf{L}}}$ is negative at the roots. For a positive trace, the corresponding root belongs to the subdominant eigenvalue ('$-$' sign in equation (3.2)), and hence, the dominant eigenvalue is positive and has no root at $k_\pm$.

[6]In the RD setting, it corresponds to the known requirement that the inhibitor diffuses faster than the activator. That is, changing the roles of $u$ and $v$ alters the condition to $\sigma<1$. If both, $f_u$ and $g_v$, are either positive or negative, a Turing instability cannot occur.

not correspond to an Allen–Cahn instability, instead the Turing band of unstable wavenumbers simply attaches to $k=0$ when $A \leq 0$.

The loci of all oscillatory instabilities, i.e. at onset with $\mathrm{Re}\,\tilde{\lambda}=0$ and frequency $\mathrm{Im}\,\tilde{\lambda}=\tilde{\omega}\neq 0$, are determined by $\mathrm{tr}\,\underline{\tilde{\mathbf{L}}}=0$, i.e. if $f_u+g_v-k^2(1+\sigma)=0$. This gives marginally stable modes with

$$k_o^2=\frac{f_u+g_v}{1+\sigma}, \tag{3.9}$$

and oscillations first occur at $k_o=0$, i.e. only a Hopf instability (table 1) is possible. Its threshold is at

$$f_u+g_v=0 \tag{3.10}$$

with $\tilde{\omega}_0=\det\underline{\tilde{\mathbf{L}}}(k=0)=A$.

Next, we compare stationary and oscillatory instabilities by considering the transition from real to complex eigenvalues. Complex eigenvalues $\tilde{\lambda}$ occur for $(\mathrm{tr}\,\underline{\tilde{\mathbf{L}}})^2-4\det\underline{\tilde{\mathbf{L}}}<0$, i.e. if

$$[f_u-g_v-(1-\sigma)k^2]^2+4f_vg_u<0. \tag{3.11}$$

Similar to the Turing instability, any oscillatory instability requires non-reciprocal interactions $f_vg_u<0$. In consequence, for $k=0$, the condition (3.11) can be reduced to

$$A>\frac{1}{4}(f_u+g_v)^2, \tag{3.12}$$

which is outside the parametric region where a large-scale stationary instability is observed ($A<0$) implying that our previous consideration on the Allen–Cahn instability applies.

For $k=k_T$, we introduce (3.6) into (3.11) and find that the eigenvalue is complex if

$$g_v-\frac{4\sigma}{1+\sigma}\sqrt{-f_vg_u}<\sigma f_u<g_v+\frac{4\sigma}{1+\sigma}\sqrt{-f_vg_u}. \tag{3.13}$$

The onset of the Turing instability (compared with (3.8)) is outside of this interval if $\sigma\neq 1$. Then our previous considerations based on real eigenvalues apply to the Turing instability as well. For the special case $\sigma=1$, complex eigenvalues occur independently of the wavenumber at $\sigma f_u=g_v\pm 2\sqrt{-\sigma f_vg_u}$. This is identical to the onset condition of the Turing instability (compared with (3.8)). Furthermore, at this specific point, one has $k_T=k_o$. Thus, the Turing instability is prohibited by complex eigenvalues if $\sigma=1$, as one would expect for an RD system with equal diffusion constants.

A codimension-two point exists if Hopf ($f_u+g_v=0$) and Turing ($\sigma f_u=g_v+2\sqrt{-\sigma f_vg_u}$) instability occur simultaneously, i.e. if

$$g_v=-f_u=-2\frac{\sqrt{-\sigma f_vg_u}}{1+\sigma} \tag{3.14}$$

and all aforementioned requirements are fulfilled, too. A typical stability diagram in the $(g_v,f_u)$-plane at fixed $f_v$, $g_u$ and $\sigma$ is given in figure 1.

Although onset conditions for linear instabilities for the two-species RD system and the corresponding non-reciprocal two-field CH model are identical, the respective dispersion relations are not. In particular, for the large-scale oscillatory instability in the conserved case, the frequency scales with $k^2$, i.e. $\omega_0=k^2\tilde{\omega}_0$. Therefore, directly at onset, the large-scale instability cannot be oscillatory as there $k_o=0$, and the conserved-Hopf instability differs from the standard Hopf instability at $f_u=-g_v$, and takes place only when a mode with the largest available wavelength becomes unstable. For a one-dimensional finite sized system with domain length $L$ and periodic boundary conditions, the available wavenumbers are $k_{L/n}=2n\pi/L$.

As a consequence of this effect, resonances only occur in the vicinity of but not directly at the codimension-two point of the infinite system. In the most interesting case, an oscillatory mode (wave) with $k_L=k_o$ and a stationary mode with the wavenumber $k_{L/n}=k_T$, where $n>1$ are simultaneously marginal. Figure 2 presents a corresponding dispersion relation with $n=2$, i.e. for the parameters marked by a cross symbol in figure 1. If one considers larger values of $n$, the position of the cross moves on the orange line closer to the codimension-two point. For specific

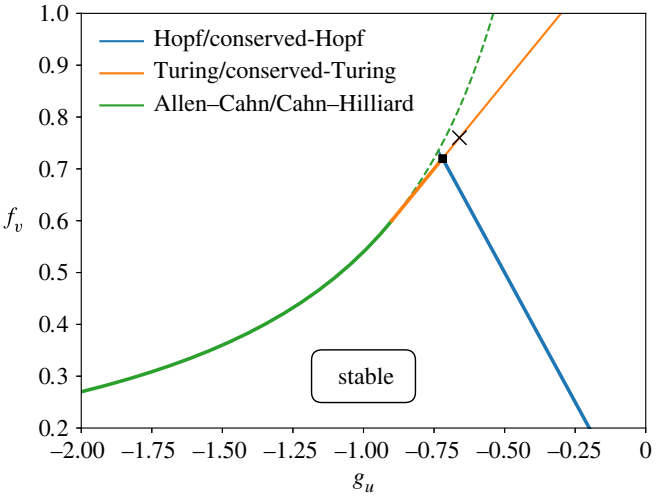


**Figure 1.** Linear stability diagrams in the $(g_v, f_u)$ plane showing the thresholds of Hopf/conserved-Hopf (homogeneous/large-scale oscillatory, equation (3.10)), Turing/conserved-Turing (small-scale stationary, equation (3.8)) and Allen–Cahn/Cahn–Hilliard (homogeneous/large-scale stationary, equation (3.5)) instabilities as blue, orange and green lines, respectively. Here, $\sigma = 1.5 > 1$ and non-reciprocity $f_v g_u = -0.54$. The focus lies in the region where $u$ is autocatalytic ($f_u > 0$) and $v$ is not ($g_v < 0$). The linearly stable region is delimited by heavy solid lines. Thin solid lines indicate where further instabilities set in beyond the dominating one. The dashed green line indicates where the already unstable Turing band reaches $k_- = 0$ (transition across orange line) or where the unstable complex eigenvalues near $k = 0$ become real (transition across blue line). The square symbol marks the codimension-two point (equation (3.14)), where Hopf/conserved-Hopf and Turing/conserved-Turing instabilities occur simultaneously. The cross symbol indicates the loci of the dispersion relation given in figure 2. (Online version in colour.)

finite systems of domain size $L \neq 2\pi n/k_T$, the relevant stationary modes are rather related to $k_-$ or $k_+$—the limiting values of the band of unstable conserved-Turing modes (compare with equation (3.4)). Close to the corresponding primary bifurcations, the behaviour can be analysed with the help of a weakly nonlinear analysis [62,63], as described in §4 for a general system (2.3). Further beyond the onset, one may compare general weakly nonlinear results with fully nonlinear time simulations for a specific conserved amended FitzHugh–Nagumo model (see §5). Note that for systems without conservation laws, resonances are frequently studied. Examples include Hopf–Turing, Turing–Turing and wave–Turing resonances in RD systems or nonlinear optical systems [62–66].

## 4. Hopf–Turing resonance—weakly nonlinear analysis

We consider the resonant interaction between a conserved-Turing and two conserved-Hopf modes with the three wavevectors forming an isosceles triangle. In a finite system, they satisfy the condition $\mathbf{k}_{o1} - \mathbf{k}_{o2} + \mathbf{k}_\pm = \mathbf{0}$ with $|\mathbf{k}_{o1}| = |\mathbf{k}_{o2}| \equiv k_o$. The corresponding interactions for a non-conserved system have been analysed in [62]. We consider the case when the resonance occurs close to the common onset of linear instability for a specific finite system, defined by the critical values of two parameters. We impose a small deviation in one of these parameters, let us say $\beta = \beta_c + \varepsilon$ with $|\varepsilon| \ll 1$. Then, both the growth rates and the amplitudes are small and, thus, by expanding them in powers of $\varepsilon$, they are treated through a weakly nonlinear approach. Details are given in appendix A, and here, we only sketch the procedure and give its results.

As an ansatz, we write the two-component vector field $\mathbf{u} = (u, v)$ as a sum of the uniform steady state $\boldsymbol{u}_s$ and a small deviation, i.e.

$$\mathbf{u} = \mathbf{u}_s + \varepsilon[a_+(T)\mathbf{u}_+ e^{i\mathbf{k}_+\cdot\mathbf{x}} + a_{o1}(T)\mathbf{u}_{o1}\, e^{i(\mathbf{k}_{o1}\cdot\mathbf{x}+\omega_{o1}t)} + a_{o2}(T)\mathbf{u}_{o2}\, e^{i(\mathbf{k}_{o2}\cdot\mathbf{x}+\omega_{o2}t)} + \text{c.c.}] + \mathcal{O}(\varepsilon^2), \quad (4.1)$$

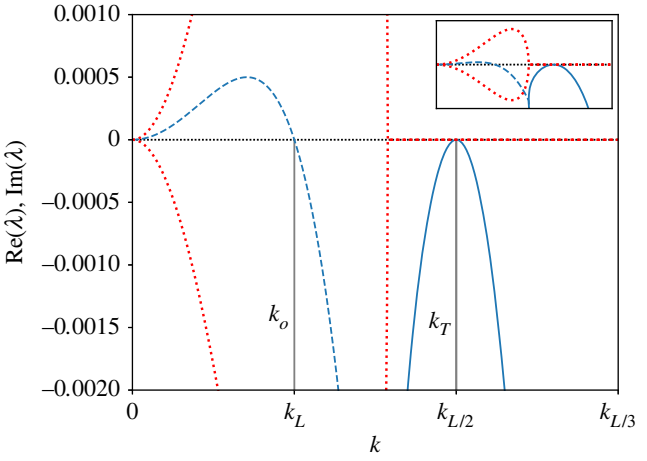


**Figure 2.** Dispersion relation showing real and imaginary part of $\lambda(k)$ (equation (3.2)) at the parameter values where the conserved-Turing instability has its onset (at $k_{L/2} = k_T$) and is resonant with the critical mode of the conserved-Hopf instability ($k_o = k_L$), i.e. $k_T = 2k_o$. Solid and dashed blue lines represent $\mathrm{Re}\,\lambda(k)$ for real and complex eigenvalues, respectively. Dotted red lines give the imaginary parts. The inset illustrates the dispersion on a larger magnitude range. Parameters are $\sigma = 1.5$, $f_u = 0.76$, $f_v = -1$, $g_u = 0.54$ and $g_v = -0.66$ and correspond to the cross symbol in figure 1. In a finite system, this resonance is only realizable for a perfectly tuned domain size of $L = 10\pi$. (Online version in colour.)

where $a_+(T)$, $a_{o1}(T)$ and $a_{o2}(T)$ are the amplitudes that evolve on a large time scale $T = \varepsilon t$; $\mathbf{u}_+ \in \mathbb{R}$ and $\mathbf{u}_{o1}, \mathbf{u}_{o2} \in \mathbb{C}$ are the zero eigenvectors of the stationary and the two wave modes, respectively. Analogously to the zero eigenvalues, they are equal in the conserved and non-conserved case. The frequencies $\omega_{o1}$ and $\omega_{o2}$ are the imaginary parts of the eigenvalues at onset of instability of the wave modes. We consider an isotropic system, which implies that $\mathbf{u}_{o1} = \mathbf{u}_{o2} \equiv \mathbf{u}_o$ and $\omega_{o1} = \omega_{o2} \equiv \omega_o$. Note that either end of the Turing-unstable wavenumber band, $\mathbf{k}_+$ or $\mathbf{k}_-$, may be used for the stationary mode. Here, we take $\mathbf{k}_+$.

After inserting equation (4.1) into equations (2.3), the leading-order amplitude equations are obtained at $\mathcal{O}(\varepsilon^2)$ by applying solvability conditions, i.e. multiplying by corresponding adjoint eigenvectors $\mathbf{u}_+^\dagger$, $\mathbf{u}_o^\dagger$ normalized to satisfy $\mathbf{u}_+^\dagger \cdot \mathbf{u}_+ = \mathbf{u}_o^\dagger \cdot \mathbf{u}_o = 1$, and projecting onto the extant Fourier modes. For details, see appendix Aa.

The general form of the resulting lowest-order resonant amplitude equations is the same as in the standard non-conserved case. However, the coefficients of these equations, which depend on the eigenvectors, the Jacobian matrix and the Hessian, carry an additional $k_+^2$ and $k_o^2$ prefactor corresponding to the respective stationary and oscillatory mode:

$$\left.\begin{aligned} &\dot{a}_+ = k_+^2(\mu_+ a_+ + \nu_+ \bar{a}_{o1} a_{o2}) \\ \text{and}\quad &\dot{a}_{o1} = k_o^2(\mu_o a_{o1} + \nu_o \bar{a}_+ a_{o2}) \quad \text{and} \quad \dot{a}_{o2} = k_o^2(\mu_o a_{o2} + \nu_o a_+ a_{o1}) \end{aligned}\right\}, \tag{4.2}$$

where $\nu_+$ is real, while $\nu_o$ is complex. The coefficient $\mu_+$ is real and, since the imaginary part of $\mu_o$ can be absorbed into the frequency of the wave modes (i.e. by applying a transformation $a_{o1/2} \to a_{o1/2}\, \mathrm{e}^{\mathrm{i}k_o^2 \,\mathrm{Im}\mu_o t}$ or equivalently $\omega_o \to \omega_o + k_o^2\,\mathrm{Im}\mu_o$), this parameter can be also viewed as real. Since the interaction coefficients are generally distinct, the system lacks gradient structure, allowing, in principle, for persistent non-stationary behaviour within the amplitude equation representation, leading to secondary oscillations of the original field. Including cubic terms is unnecessary close to the onset, since the amplitudes may remain finite in this system even without higher-order damping interactions.

By using the polar representation of the complex amplitudes, $a_+ = \rho_+ \mathrm{e}^{\mathrm{i}\theta_+}$, $a_{o1} = \rho_1 \mathrm{e}^{\mathrm{i}\theta_1}$ and $a_{o2} = \rho_2 \mathrm{e}^{\mathrm{i}\theta_2}$, (4.2) is written in terms of the three real positive amplitudes and three phases, but the

dynamics depends only on the single-phase combination $\Theta = \theta_+ + \theta_1 - \theta_2$, so that (4.2) can be reduced to a system of four real equations as described in appendix Aa:

$$\left.\begin{aligned} &\dot{\rho}_+ = -\rho_+ + \rho_1\rho_2 \cos\Theta \\ \text{and}\quad &\dot{\rho}_1 = \mu\rho_1 + \rho_+\rho_2 \cos(\Theta - \varphi) \quad \text{and} \quad \dot{\rho}_2 = \mu\rho_2 + \rho_+\rho_1 \cos(\Theta + \varphi) \end{aligned}\right\} \tag{4.3}$$

and

$$\dot{\Theta} = -\frac{\rho_1\rho_2}{\rho_+}\sin\Theta - \rho_+\left[\frac{\rho_1}{\rho_2}\sin(\Theta + \varphi) + \frac{\rho_2}{\rho_1}\sin(\Theta - \varphi)\right]. \tag{4.4}$$

The only remaining effective parameters are $\mu = \mu_o k_o^2/(|\mu_+|k_+^2)$, and $\varphi$ as the phase of the complex parameter $\nu_o$.

This system of equations has stationary and oscillatory solutions summarized in figure 3. In the stationary case, the values of the amplitudes $\rho_+, \rho_1, \rho_2$ obtained by resolving (4.3) are (see appendix Ab for details)

$$\rho_+ = \frac{|\mu|}{[\cos(\Theta - \varphi)\cos(\Theta + \varphi)]^{1/2}} \quad \text{and} \quad \rho_{1,2} = \left[-\frac{\mu}{\cos(\Theta \pm \varphi)\cos\Theta}\right]^{1/2}. \tag{4.5}$$

Introducing (4.5) into (4.4) brings the equation defining stationary values of $\Theta$ into the form

$$-\tan\Theta + \mu[\tan(\Theta - \varphi) + \tan(\Theta + \varphi)] = 0. \tag{4.6}$$

A trivial solution to (4.6) is $\Theta = 0$, which defines the symmetric stationary solution of (4.3) with $\rho_+ = \rho_1^2 = \rho_2^2 = |\mu/\cos\varphi|$. This state corresponds in the original model to a steady pattern with a superposed standing wave giving the impression of a mass oscillating between two neighbouring peaks (for a visual impression in the one-dimensional set-up, see figure 3*l*). Related localized patterns with a superposed oscillation on a larger scale are also found in a non-reciprocal CH model [36]. In active phase-field crystal models, related states are described as alternating localized or alternating periodic states [43].

An asymmetric stationary solution is obtained when (4.6) is converted through a chain of trigonometric transformations (see appendix Ab) into a transparent implicit relation

$$(1 - 2\mu)\cos^2\Theta = \sin^2\varphi. \tag{4.7}$$

Hence, the asymmetric solution is confined to the interval $0 \le \mu \le \frac{1}{2}\cos^2\varphi$. The existence limits correspond to the bifurcation from the trivial state at $\mu = 0$ and the pitchfork bifurcation from the symmetric solution at $\mu = \frac{1}{2}\cos^2\varphi$. An additional restriction comes from the condition that the amplitudes given by (4.5) have to be real and positive. This requires $|\varphi| > \pi/2$. Branches of solutions do not diverge if $|\Theta| < \varphi - \pi/2$.

The asymmetric state corresponds in the original model to a pattern with a superposed travelling wave of half the wavenumber giving the impression of mass unidirectionally travelling between peaks (figure 3*k*). The asymmetric state is stable beyond the pitchfork bifurcation of the symmetric solution and undergoes a Hopf bifurcation on another stability limit. Note that this is a secondary bifurcation on top of the Hopf bifurcation creating the linearly growing wave modes involved in this planform. In the original model, this Hopf bifurcation results in a state corresponding to a standing wave with a superposed travelling modulated wave (figure 3*h–j*). To our knowledge, such states have not yet been systematically studied in systems with conservation laws although some states of similar complexity are described for an active phase-field-crystal model for a mixture of active and passive particles [43]. The instability limits of both symmetric and asymmetric stationary solutions merge at the double zero singularity located at $\varphi = \frac{3}{4}\pi, \mu = \frac{1}{4}$. Further details, involving elaborate calculations, are given in appendix Ac.

The pitchfork bifurcation corresponds in the original model to a kind of drift-pitchfork bifurcation. Related localized patterns with superposed oscillation and drift are also found in a particular non-reciprocal CH model [36] and in active phase-field-crystal models [42,43]. Note

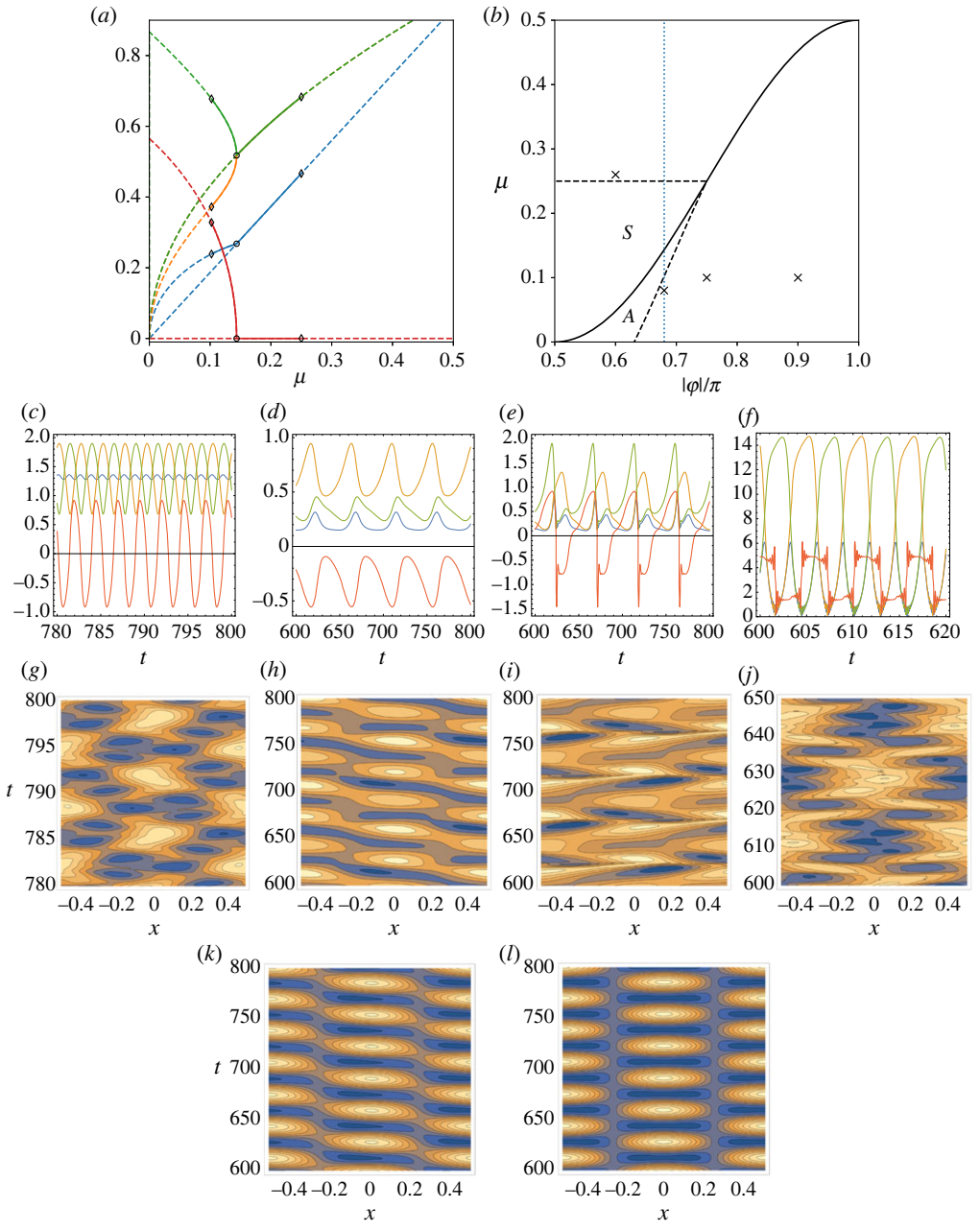


**Figure 3.** Results of the weakly nonlinear analysis are presented: (*a*) Branches of stationary solutions at $\varphi = 0.68\pi$ as a function of $\mu$. Diamond and circle symbols indicate Hopf and pitchfork bifurcations. Stable and unstable branches of solutions are shown by the solid and dashed lines, respectively. (*b*) Phase diagram with solid and dashed lines indicate pitchfork and Hopf bifurcations, respectively. The regions of prevailing stationary linearly stable symmetric and asymmetric states are indicated by the letters '*S*' and '*A*', respectively. (*c–f*) Amplitudes as functions of time for different types of long-time oscillatory behaviour. The parameters are (*c*) $\mu = 0.26$, $\varphi = 0.6\pi$, (*d*) $\mu = 0.08$, $\varphi = 0.68\pi$, (*e*) $\mu = 0.1$, $\varphi = 0.75\pi$ and (*f*) $\mu = 0.1$, $\varphi = 0.9\pi$, and are indicated by cross symbols in (*b*). In (*a*,*c–f*), the curves for $\rho_+$, $\rho_1$, $\rho_2$ and $\Theta$ are shown as blue, orange, green and red lines, respectively. (*g–l*) Space-time plots in the specific one-dimensional set-up of the original field given by $u(x, t) = \rho_+ \cos(k_+ x + \Theta(t)) + \rho_1 \cos(k_o x + \omega t) + \rho_2 \cos(-k_o x + \omega t)$ with $k_+ = 2k_o = 4\pi/L$ with domain size $L = 1$ and (*g*) $\omega = 1$, (*h–l*) $\omega = 0.2$. (*g*) to (*j*) correspond to the oscillating states of (*c*) to (*f*). (*k*,*l*) correspond to the linearly stable asymmetric state at $\mu = 0.12$, $\varphi = 0.68\pi$ and the linearly stable symmetric state at $\mu = 0.2$, $\varphi = 0.68\pi$, respectively. (Online version in colour.)

that, due to the resonance, the described complex scenario differs from the basic codimension-one scenario where a steady state starts to drift at a drift-pitchfork [67] or drift-transcritical [14] bifurcation (all called travelling bifurcation in [58]). It is more closely related to scenarios where a stable standing wave that emerged in a Hopf bifurcation gives way to a modulated travelling wave through a drift-pitchfork bifurcation or where a stationary state that is unstable to a drift mode undergoes an additional Hopf bifurcation [38,68]. These scenarios are slightly simpler than the one treated here as they do not involve a spatial resonance. A small deviation from the resonance conditions could also result in such scenarios. This is, however, not captured by the amplitude equations.

Figure 3*a* presents a bifurcation diagram showing the stationary solution branches given by (4.5) and (4.7) for fixed $\varphi = 0.68\pi$, where the coloured lines give the three different amplitudes and the phase as described in the caption. A linear stability analysis of the symmetric state gives $[\frac{1}{2}\cos^2\varphi, \frac{1}{4}]$ as the $\mu$-range of linear stability limited by the aforementioned pitchfork bifurcation on the left-hand border (circle symbols) and a Hopf bifurcation (diamond symbols) on the right-hand border. The latter represents another secondary Hopf bifurcation, and for a visual impression of the resulting oscillatory state in the one-dimensional set-up, see figure 3*g*.

The discussed existence and linear stability in the $(\varphi, \mu)$-plane are summarized in figure 3*b*. The pitchfork bifurcation indicated by the circle symbols in 3*a* is given as the solid line that separates the regions '*A*' and '*S*', where the asymmetric and symmetric stationary solutions are linearly stable, respectively. The stability regions are further limited by the dashed lines that mark the loci of the Hopf bifurcations given by diamond symbols in 3*a*. Examples of corresponding periodic orbits obtained in the description of the amplitude equations are shown in figure 3*c–f* in the sequence of increasing $\varphi$; their loci in the $(\varphi, \mu)$-plane are marked by crosses in figure 3*b*. We have to be warned that the existence region of oscillatory solutions does not encompass the entire domain where stationary solutions are unstable, since, in the absence of cubic and higher-order damping terms that could be detected by a higher-order bifurcation analysis, some trajectories escape to infinity.

## 5. Example: modified FitzHugh–Nagumo system

Next, we aim at identifying resonant behaviour in the fully nonlinear regime. To do so, we have to focus on a specific non-reciprocal CH system. We employ for this purpose a simple representative example obtained by choosing $f$ and $g$ in equations (2.3) to be of the third order in intraspecies interactions and linear in interspecies interaction. In particular, we use $f(u,v) = u - u^3 - v$ and $g(u,v) = \alpha u - \beta v - v^3$. Correspondingly, $\chi(u,v) = -u^2/2 + u^4/4 + \beta v^2/(2\gamma) + v^4/(4\gamma) + (1 - \alpha/\gamma)uv/2$ in (2.2) as well as $\mu_u^{\mathrm{nv}} = (1 + \alpha/\gamma)v/2$ and $\mu_v^{\mathrm{nv}} = -(1 + \alpha/\gamma)u/2$. Both species have non-zero mean densities, i.e., $1/L\int u\,\mathrm{d}x = u_s$ and $1/L\int v\,\mathrm{d}x = v_s$ that act as effective quadratic nonlinearities in $f$ and $g$, respectively.[7] In the absence of the cubic nonlinearity in $g$, our example represents a fully mass-conserving version of the standard FitzHugh–Nagumo model. It represents a simple example of (2.3); however, as explained later, here we have not detected the secondary Hopf instabilities and the corresponding oscillatory behaviour discussed in the previous section. Therefore, we include the cubic nonlinearity in $g$ and obtain a conserved modified FitzHugh–Nagumo system that is identical to the recently considered non-reciprocal CH model.

For the homogeneous state $(u,v) = (u_s, v_s)$ we have $f_u = 1 - 3u_s^2, f_v = -1, g_v = -(\beta + 3v_s^2)$, $g_u = \alpha, A = \alpha - (1 - 3u_s^2)(\beta + 3v_s^2), B = (1 - 3u_s^2)\sigma - (\beta + 3v_s^2)$. Imposing $3u_s^2 < 1, \beta + 3v_s^2 > 0$, we choose $u$ but not $v$ to be autocatalytic ($f_u > 0$, $g_v < 0$). If the coupling is non-reciprocal ($f_v g_u < 0$),

[7] In other words, if we introduce the shifted densities $u - u_s$ and $v - v_s$, the resulting nonlinear terms in the shifted densities include quadratic nonlinearities.

i.e. for $\alpha > 0$, the necessary conditions for the instabilities are as follows:

$$\left.\begin{aligned} &\text{Cahn-Hilliard: } A < 0 \Rightarrow \alpha < (1-3u_s^2)(\beta + 3v_s^2) \\ &\text{conserved-Turing: } B > 0 \wedge \sigma > 1 \wedge \sigma f_u > g_v + 2\sqrt{-\sigma f_v g_u} \\ &\qquad \Rightarrow \sigma > 1 \wedge \sigma(1-3u_s^2-3v_s^2) > \beta > -\sigma(1-3u_s^2-3v_s^2) + 2\sqrt{\sigma\alpha} \\ &\text{and conserved-Hopf: } A > \frac{1}{4}(f_u+g_v)^2 \wedge f_u + g_v > 0 \\ &\qquad \Rightarrow \beta < \min\left\{-1+3u_s^2-3v_s^2+2\sqrt{\alpha}, 1-3u_s^2-3v_s^2\right\} \wedge \alpha > \left(\frac{1-3u_s^2}{2}\right)^2. \end{aligned}\right\} \tag{5.1}$$

The wavenumbers of stationary and oscillatory marginal modes (compared with (3.4) and (3.9)) are then given by

$$k_\pm^2 = k_T^2\left[1 \pm \sqrt{1 - \frac{4\sigma(\alpha - (1-3u_s^2)(\beta+3v_s^2))}{\left((1-3u_s^2)\sigma - (\beta+3v_s^2)\right)^2}}\right] \tag{5.2}$$

and

$$k_o^2 = \frac{1-3u_s^2-(\beta+3v_s^2)}{1+\sigma}, \tag{5.3}$$

where $k_T^2 = ((1-3u_s^2)\sigma - (\beta+3v_s^2))/2\sigma$ is the critical wavenumber at the onset of the conserved-Turing instability.

We consider now a scenario where a marginal conserved-Hopf mode ($k_o = k_L$) and a marginal conserved-Turing mode ($k_\pm = k_{L/2}$) are resonant in a one-dimensional domain. For the considered specific system, this is achieved at $4k_o^2 = k_+^2 = k_{L/2}^2$. Using equations (5.2) and (5.3) gives after simplification the critical values

$$\left.\begin{aligned} \alpha_c &= \left(1-3u_s^2-\frac{16\pi^2}{L^2}\right)\left(1-3u_s^2-\frac{4\pi^2}{L^2}(1-3\sigma)\right) \\ \text{and}\quad \beta_c &= 1-3(u_s^2+v_s^2)-\frac{4\pi^2}{L^2}(1+\sigma), \end{aligned}\right\} \tag{5.4}$$

which define this codimension-two point. The corresponding frequency of the marginal conserved-Hopf mode is

$$\omega_o = \frac{8\sqrt{3}\pi^3\sqrt{L^2(\sigma-1)(3u_s^2-1)+4\pi^2(4\sigma-1)}}{L^4}. \tag{5.5}$$

To consider the weakly nonlinear regime in the vicinity of the codimension-two point, we set $\alpha = \alpha_c$ and $\beta = \beta_c + \varepsilon$. The resulting relevant non-zero entries of $\partial\underline{\mathbf{L}}(k^2)/\partial\beta$ and the Hessian $\underline{\underline{\mathbf{H}}}$ that implicitly enter equations (4.2) (see appendix Aa for details) are as follows:

$$\left.\begin{aligned} &\frac{\partial L_{22}(k^2)}{\partial\beta} = -k^2, \qquad H_{111}(k^2) = k^2 f_{uu} = -k^2 6u_s \\ &\text{and}\quad H_{222}(k^2) = k^2 g_{vv} = -k^2 6v_s. \end{aligned}\right\} \tag{5.6}$$

Note that for the special case of a trivial homogeneous state, i.e. $u_s = v_s = 0$, quadratic interactions are absent and the description of resonances via the leading order amplitude equations (4.2) do not apply.

Incorporating the imaginary part of $\mu_o$ into the frequency, the coefficients in equations (4.2) become

$$\left.\begin{aligned} \mu_+ &= \varepsilon \frac{L^2(1-3u_s^2)-16\pi^2}{12\pi^2(\sigma+1)}, \quad \mu_o = -\frac{\varepsilon}{2} \\ \text{and} \qquad \nu_+ &= \frac{L^2\,(v_s-u_s(3u_sv_s+1))-16\pi^2 v_s}{2\pi^2(\sigma+1)}, \\ \text{and} \qquad \nu_o &= \frac{3L^2u_s}{L^2(3u_s^2-1)+16\pi^2} - 3v_s + \mathrm{i}\frac{12\pi^2\left(L^2(3u_s^2-1)+4\pi^2\right)\left(L^2(3u_s^2v_s+u_s-v_s)+16\pi^2v_s\right)}{\left(L^2(3u_s^2-1)+16\pi^2\right)L^4\omega_o}. \end{aligned}\right\} \tag{5.7}$$

We have performed direct time simulations of this model in the vicinity of the degenerate bifurcation where we expect resonance behaviour. In particular, we choose $\mu_o > 0$ and $\mu_+ < 0$ as in §4, i.e. we decrease $\beta$ by $\varepsilon < 0$. Fixing a specific domain size $L$, there are $\sigma, u_s$ and $v_s$ as free parameters of the original model that can be used to adjust three parameters of equations (5.7). To compare the specific model with the weakly nonlinear results in figure 3 (from equations (4.3) and (4.4)), we adjust $\mu = \mu_o k_o^2/(|\mu_+|k_+^2)$, and $\varphi$ as the phase of the complex parameter $\nu_o$. As there is an additional free parameter in the original model, we have further fixed the absolute value of $\nu_o$ to one. Note that in the absence of a cubic nonlinearity in $g(u,v)$, i.e. for the fully mass-conserving version of the standard FitzHugh–Nagumo model, $H_{222}(k^2)$ in equation (5.6) vanishes and $v_s$ does not contribute to the coefficients in equations (5.7). In principle, there are still enough free parameters to adjust $\mu$ and $\varphi$, practically however, we are unable to enter the parameter range where we expect oscillatory states, i.e. the range depicted in figure 3*b*. This is due to further restrictions based on the various inequalities involved in the occurrence of the instabilities (compare with equations (5.1)) and the considered signs in the amplitude equations (4.3) and (4.4) (compare with appendix Aa). Including the cubic nonlinearity in $g(u,v)$ solves this issue. A typical result is given in figure 4, where (*a*) gives the dispersion relation at parameter values where $k_o = k_L$ and $k_+ = k_{L/2}$ are resonant, while (*b*) shows a space-time plot of the corresponding time simulation. The latter indeed shows a two-frequency behaviour analogous to the secondary oscillations found with the weakly nonlinear approach in §4 (compare with figure 3).

However, performing time simulations at parameters that correspond to regions '*A*' and '*S*' in figure 3*b*, where asymmetric and symmetric stationary solutions of the amplitude equations (4.2) are, respectively, stable, we encounter only travelling waves, standing waves (both with wavenumber $k_L$) or stationary Turing patterns with the wavenumber $k_{L/2}$. Due to the scaling in the employed ansatz (4.1), these states are not captured by the amplitude equations.

## 6. Summary and outlook

We have considered a non-reciprocally coupled two-field CH system that is known to allow for oscillatory behaviour and suppression of coarsening. We have reviewed the linear stability analysis of uniform steady states and have shown that for general intraspecies and interspecies interaction terms all instability thresholds of the fully mass-conserving CH system are identical to the ones for the corresponding non-mass-conserving RD system. Next, we have briefly highlighted the differences in the linear behaviour of conserved and non-conserved models that occur beyond the instability onset. Focusing on the codimension-two point where conserved-Hopf and conserved-Turing instabilities simultaneously occur, we have discussed possible interactions of linear modes. In particular, we have analysed the specific case of a 'Hopf–Turing' resonance. To do so, we have first employed a weakly nonlinear approach to consider the amplitude equations close to the codimension-two point. After discussing the behaviour of solutions in the general case, we have derived the coefficients of the amplitude equations for a specific non-reciprocal CH model that corresponds to a modified conserved FitzHugh–Nagumo model. Although a conserved version of the standard FitzHugh–Nagumo model shows a codimension-two point, it does not allow to adjust parameters in such a way that the parameter

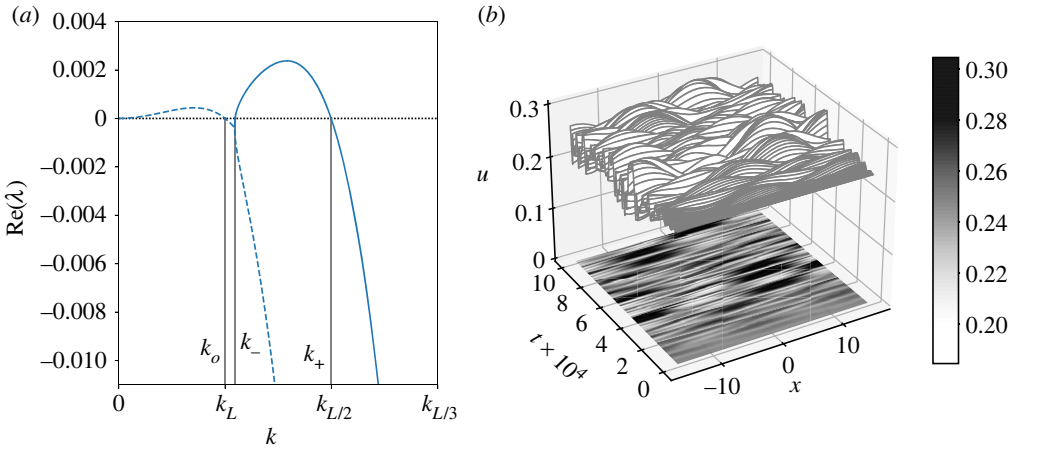


**Figure 4.** (*a*) Dispersion relation $\mathrm{Re}\,\lambda(k)$ (equation (3.2)) for a finite system of the size $L$ at parameter values where there are resonant marginal modes $k_o = k_L$ (equation (3.9)) and $k_+ = k_{L/2}$ (equation (3.4)) of the conserved-Hopf and conserved-Turing instabilities, respectively. (*b*) Space-time plot of $u(x, t)$ obtained by fully nonlinear time simulation of the mass-conserving modified FitzHugh–Nagumo system showing two-frequency oscillatory behaviour. The parameters are $\sigma \approx 1.19557 > 1$, $f_u[= 1 - 3u_s^2] \approx 0.81867, f_v = -1, g_u[= \alpha] \approx 0.60739$ and $g_v[= -\beta - 3v_s^2] \approx -0.73075$, where for the specific model $\beta = \beta_c + \varepsilon \approx 0.15016$ with $\varepsilon = -10^{-4}, u_s \approx 0.24585$ and $v_s \approx 0.43992$. The domain size is $L = 10\pi$. In the formulation of the amplitude equations (4.3) and (4.4), the corresponding parameters are $\mu = 0.05$ and $\varphi = -0.65\pi$, respectively. (Online version in colour.)

ranges of the weakly nonlinear model correspond to the interesting cases shown in figure 3*b*. This may be due to the fact that it is a non-generic model, see discussion in [9]. Finally, we have shown that fully nonlinear time simulations indeed show two-frequency behaviour analogous to the secondary oscillations discussed in the framework of the weakly nonlinear theory.

However, we have also noted that not all behaviour predicted by the amplitude equation is found in the fully nonlinear calculation. To better understand where weakly and fully nonlinear results agree and where they disagree, the mapping of the respective parameter sets and resulting behaviour should be further scrutinized in the future. A problem that needs further attention is that the parameter mapping is not one-to-one and itself is highly nonlinear. This makes it, for instance, quite difficult to identify parameter ranges where certain states dominate in a nonlinear model with corresponding ranges in the weakly nonlinear description. The usage of continuation methods might allow one to obtain bifurcation diagrams for nonlinear models that could then be directly compared with a bifurcation diagram presented in the weakly nonlinear case. This would also allow one to clarify the question whether an additional inclusion of cubic terms into the weakly nonlinear approach has a major impact.

Data accessibility. Mathematica codes that support the weakly nonlinear analysis are published at Zenodo http://doi.org/10.5281/zenodo.7503482 [69].

Authors' contributions. T.F.: conceptualization, data curation, formal analysis, investigation, methodology, software, validation, visualization, writing—original draft and writing—review and editing; U.T.: conceptualization, formal analysis, investigation, methodology, supervision, validation, writing—original draft and writing—review and editing; L.M.P.: conceptualization, formal analysis, investigation, methodology, supervision, validation, writing—original draft and writing—review and editing.

All authors gave final approval for publication and agreed to be held accountable for the work performed therein.

Conflict of interest declaration. We declare we have no competing interests.

Funding. T.F.H. was supported by the foundation 'Studienstiftung des deutschen Volkes'. T.F.H. and U.T. acknowledge support from the doctoral school 'Active Living Fluids' funded by the German-French University (grant no. CDFA-01-14).

Acknowledgements. The authors thank Svetlana V. Gurevich for fruitful discussions.

# Appendix A. Details of weakly nonlinear analysis

## (a) Derivation of the amplitude equations (4.3) and (4.4)

In this section, we provide more details on the calculations discussed in §4. We consider the system (2.3) close to a wave-Turing resonance, where the three wavevectors form an isosceles triangle. The steady state is denoted by $\mathbf{u}_s$. In one spatial dimension (1D), the 'triangle' is flat and the wavenumber of the oscillatory mode is simply half the wavenumber of the stationary one. To be definite, we concentrate here on this case, though all derivations apply to a general situation. To capture nonlinear interactions by a weakly nonlinear approach, we further demand that both corresponding growth rates are small, i.e. we are close to the codimension-two bifurcation that occurs in an infinite system under the conditions given by equation (3.14). In a specific finite-size system of length $L$, the condition is modified to $2k_o = k_+ = k_{L/2} = 4\pi/L$, where $k_o$ (equation (3.9)) and $k_+$ (equation (3.4)) correspond to the marginal modes of the conserved-Hopf and the conserved-Turing instability, respectively. Note that the following results equivalently apply if one chooses the stationary marginal mode with $k_-$ instead of $k_+$ to be in resonance with the oscillatory ones. The two conserved-Hopf modes correspond to left and right-travelling waves in 1D. In an isotropic system, they exhibit the same dispersion, i.e. they have the same frequency and the same eigenvector. Two parameters have to be set to specific critical values that adjust the codimension-two point. Then, we use one of them, say $\beta$, and introduce a small deviation, i.e. $\beta = \beta_c + \varepsilon$. Since $\varepsilon \ll 1$, it can be used as a smallness parameter, and we expand all fields in $\varepsilon$ as follows:

$$\left.\begin{aligned} \mathbf{u} &= \mathbf{u}_s + \varepsilon \mathbf{u}_1(x,t,T) + \varepsilon^2 \mathbf{u}_2(x,t,T) + \mathcal{O}(\varepsilon^3) \\ \text{with } \mathbf{u}_1(x,t,T) &= a_+(T)\mathbf{u}_+ \mathrm{e}^{\mathrm{i}k_+ x} + a_{o1}(T)\mathbf{u}_o \mathrm{e}^{\mathrm{i}(-k_o x+\omega_o t)} + a_{o2}(T)\mathbf{u}_o \mathrm{e}^{\mathrm{i}(k_o x+\omega_o t)} + \text{c.c.} \end{aligned}\right\} \tag{A 1}$$

The amplitudes $a_+(T)$, $a_{o1}(T)$ and $a_{o2}(T)$ evolve on a large time scale $T = \varepsilon t$ and correspond to the stationary, right-travelling and left-travelling mode, respectively, with their corresponding zero eigenvectors $\mathbf{u}_+ \in \mathbb{R}$ and $\mathbf{u}_o \in \mathbb{C}$. The frequency $\omega_o > 0$ is the imaginary part of the eigenvalues at the onset of instability of the wave modes. Note that equation (A 1) results from the more general ansatz (4.1) if isotropy is used. We introduce (A 1) into (2.3) and expand in $\varepsilon$ to obtain

$$\varepsilon^2(\partial_T \mathbf{u}_1(x,t,T) + \underline{\mathcal{L}} \cdot \mathbf{u}_2(x,t,T)) + \mathcal{O}(\varepsilon^3) = \varepsilon^2 \left( \frac{\partial \underline{\mathbf{L}}}{\partial \beta}(\beta - \beta_c) \cdot \mathbf{u}_1 + \mathbf{u}_1 \cdot \underline{\underline{\mathbf{H}}} \cdot \mathbf{u}_1 \right) + \mathcal{O}(\varepsilon^3), \tag{A 2}$$

where

$$\underline{\mathcal{L}} = \underline{\mathbf{1}}\partial_t - \underline{\mathbf{L}} = \underline{\mathbf{1}}\partial_t + \partial_{xx} \begin{pmatrix} \partial_{xx} + f_u & f_v \\ g_u & \partial_{xx} + g_v \end{pmatrix} \tag{A 3}$$

is the linear partial differential operator that includes both the time derivative with respect to the fast time scale $t$ and the Jacobian matrix $\underline{\mathbf{L}}$, written here in spatial representation. $\underline{\mathbf{1}}$ is the unit matrix and the zero eigenmodes solve

$$\underline{\mathcal{L}} \cdot \mathbf{u}_+ \mathrm{e}^{\mathrm{i}k_+ x} = \underline{\mathcal{L}} \cdot \mathbf{u}_o \mathrm{e}^{\mathrm{i}(\pm k_o x + \omega_o)} = \mathbf{0}. \tag{A 4}$$

Further, we define the Hessian $\underline{\underline{\mathbf{H}}} = \nabla_{\mathbf{u}} \underline{\mathbf{L}}$. Both $\underline{\mathcal{L}}$ and $\underline{\underline{\mathbf{H}}}$ are evaluated for the uniform steady state $\mathbf{u} = \mathbf{u}_s$ at $\beta = \beta_c$. The special property of the Hopf–Turing resonance is that quadratic terms are sufficient to obtain a saturated system, so that, for our purpose, we neglect all higher terms. Next, we multiply the remaining $\mathcal{O}(\varepsilon^2)$ terms in equation (A 2) by one of the three adjoint linear modes that solve the adjoint linear eigenvalue problem, i.e.

$$\mathbf{u}_+^\dagger \mathrm{e}^{-\mathrm{i}k_+ x} \cdot \underline{\mathcal{L}} = \mathbf{u}_o^\dagger \mathrm{e}^{-\mathrm{i}(\pm k_o x + \omega_o)} \cdot \underline{\mathcal{L}} = \mathbf{0}, \tag{A 5}$$

and integrate over the whole domain. In each case, the term that involves $\mathbf{u}_2$ in equation (A 2) vanishes, and the integration amounts to a projection on the corresponding Fourier modes. We

normalize all adjoint vectors via $\mathbf{u}_+^\dagger \cdot \mathbf{u}_+ = \mathbf{u}_o^\dagger \cdot \mathbf{u}_o = 1$. This gives

$$\left.\begin{aligned} \mathrm{e}^{\mathrm{i}k_+ x} \sim \partial_T a_+ &= \mathbf{u}_+^\dagger \cdot \frac{\partial \underline{\mathbf{L}}(k_+^2)}{\partial \beta} \cdot \mathbf{u}_+ (\beta - \beta_c) a_+ + \mathbf{u}_+^\dagger \cdot (\bar{\mathbf{u}}_o \cdot \underline{\underline{\mathbf{H}}}(k_+^2) \cdot \mathbf{u}_o) \bar{a}_{o1} a_{o2}, \\ \mathrm{e}^{\mathrm{i}(-k_o x + \omega_o t)} \sim \partial_T a_{o1} &= \mathbf{u}_o^\dagger \cdot \frac{\partial \underline{\mathbf{L}}(k_o^2)}{\partial \beta} \cdot \mathbf{u}_o (\beta - \beta_c) a_{o1} + \mathbf{u}_o^\dagger \cdot (\mathbf{u}_+ \cdot \underline{\underline{\mathbf{H}}}(k_o^2) \cdot \mathbf{u}_o) \bar{a}_+ a_{o2}, \\ \text{and} \qquad \mathrm{e}^{\mathrm{i}(k_o x + \omega_o t)} \sim \partial_T a_{o2} &= \mathbf{u}_o^\dagger \cdot \frac{\partial \underline{\mathbf{L}}(k_o^2)}{\partial \beta} \cdot \mathbf{u}_o (\beta - \beta_c) a_{o2} + \mathbf{u}_o^\dagger \cdot (\mathbf{u}_+ \cdot \underline{\underline{\mathbf{H}}}(k_o^2) \cdot \mathbf{u}_o) a_+ a_{o1}, \end{aligned}\right\} \tag{A 6}$$

where we use the resonance condition

$$\mathrm{e}^{\mathrm{i}k_+ x}\, \mathrm{e}^{\mathrm{i}(-k_o x + \omega_o t)} = \mathrm{e}^{\mathrm{i}((k_+ - k_o)x + \omega_o t)} = \mathrm{e}^{\mathrm{i}(k_o x + \omega_o t)}, \tag{A 7}$$

which gives the quadratic coupling terms. All quantities with a bar denote complex conjugates. In the resulting system of amplitude equations (A 6), all spatial derivatives are replaced by the corresponding wavenumber. Then equations (A 6) are rewritten as follows:

$$\left.\begin{aligned} \dot{a}_+ &= k_+^2 (\mu_+ a_+ + \nu_+ \bar{a}_{o1} a_{o2}), \\ \dot{a}_{o1} &= k_o^2 (\mu_o a_{o1} + \nu_o \bar{a}_+ a_{o2}) \quad \text{and} \quad \dot{a}_{o2} = k_o^2 (\mu_o a_{o2} + \nu_o a_+ a_{o1}), \end{aligned}\right\} \tag{A 8}$$

where the coefficients $\mu_+, \nu_+ \in \mathbb{R}$ and $\mu_o, \nu_o \in \mathbb{C}$ resemble the structure of the amplitude system in the non-conserved case [62], but in the conserved case, additional prefactors consisting of squared wavenumbers occur. We apply the transformation $\tilde{a}_{o1/2} = a_{o1/2}\, \mathrm{e}^{-\mathrm{i}k_o^2 \mathrm{Im} \mu_o t}$, i.e.

$$\dot{\tilde{a}}_{o1/2} = (\dot{a}_{o1/2} - \mathrm{i}k_o^2 \mathrm{Im}\ \mu_o a_{o1/2})\, \mathrm{e}^{-\mathrm{i}k_o^2 \mathrm{Im}\ \mu_o t}, \tag{A 9}$$

which eliminates the contribution of the imaginary part of $\mu_o$ in equations (A 8). In the following, we omit the tilde, and consider $\mu_o$ as real. Next, we introduce a polar representation of the complex amplitudes, $a_+ = \rho_+ \mathrm{e}^{\mathrm{i}\theta_+}, a_{o1} = \rho_1 \mathrm{e}^{\mathrm{i}\theta_1}, a_{o2} = \rho_2 \mathrm{e}^{\mathrm{i}\theta_2}$ and of the remaining complex coefficient $\nu_o = \nu \mathrm{e}^{\mathrm{i}\varphi}$ where, by construction, $\rho_+, \rho_1, \rho_2, \nu > 0$. Then equations (A 8) become

$$\left.\begin{aligned} (\dot{\rho}_+ + \mathrm{i}\dot{\theta}_+) \mathrm{e}^{\mathrm{i}\theta_+} &= k_+^2 (\mu_+ \rho_+ \mathrm{e}^{\mathrm{i}\theta_+} + \nu_+ \rho_1 \rho_2 \mathrm{e}^{\mathrm{i}(\theta_2 - \theta_1)}), \\ (\dot{\rho}_1 + \mathrm{i}\dot{\theta}_1) \mathrm{e}^{\mathrm{i}\theta_1} &= k_o^2 (\mu_o \rho_1 \mathrm{e}^{\mathrm{i}\theta_1} + \nu \rho_+ \rho_2 \mathrm{e}^{\mathrm{i}(-\theta_+ + \theta_2 + \varphi)}) \\ \text{and} \qquad (\dot{\rho}_2 + \mathrm{i}\dot{\theta}_2) \mathrm{e}^{\mathrm{i}\theta_2} &= k_o^2 (\mu_o \rho_2 \mathrm{e}^{\mathrm{i}\theta_2} + \nu \rho_+ \rho_1 \mathrm{e}^{\mathrm{i}(\theta_+ + \theta_1 + \varphi)}). \end{aligned}\right\} \tag{A 10}$$

We divide by the respective exponential factor on each left-hand side and introduce the relative phase $\Theta = \theta_+ + \theta_1 - \theta_2$ that can be identified as the only relevant phase information that enters the dynamics. The real and imaginary parts of equations (A 10) give the dynamics of the corresponding real amplitude and phase, respectively. Further, the dynamics of the phases are combined to give $\dot{\Theta}$. Then the amplitude equations of the relevant field quantities are as follows:

$$\left.\begin{aligned} \dot{\rho}_+ &= k_+^2 (\mu_+ \rho_+ + \nu_+ \rho_1 \rho_2 \cos \Theta), \\ \dot{\rho}_1 &= k_o^2 (\mu_o \rho_1 + \nu \rho_+ \rho_2 \cos(\Theta - \varphi)), \\ \dot{\rho}_2 &= k_o^2 (\mu_o \rho_2 + \nu \rho_+ \rho_1 \cos(\Theta + \varphi)), \\ \text{and} \qquad \dot{\Theta} = \dot{\theta}_+ + \dot{\theta}_1 - \dot{\theta}_2 &= -k_+^2 \nu_+ \frac{\rho_1 \rho_2}{\rho_+} \sin \Theta - \nu k_o^2 \rho_+ \left( \frac{\rho_1}{\rho_2} \sin(\Theta + \varphi) + \frac{\rho_2}{\rho_1} \sin(\Theta - \varphi) \right). \end{aligned}\right\} \tag{A 11}$$

It follows from the first equation in (A 11) that it is necessary for the existence of stationary solutions that either $\mu_+$ and $\nu_+$ have the same sign and $\cos \Theta < 0$, i.e. $|\Theta| > \pi/2$ or they have opposite sign, implying $\cos \Theta > 0$, i.e. $|\Theta| < \pi/2$. Here, we assume $\nu_+ > 0, \mu_+ < 0$, the latter implying that the Turing mode is linearly weakly damped. We apply a rescaling to eliminate

all but two effective parameters. Specifically, we use $1/(k_+^2|\mu_+|)$ as the time scale, $|\mu_+|k_+^2/(\nu k_o^2)$ as the scale of $\rho_+$ and $|\mu_+|k_+/(\sqrt{\nu\nu_+}k_o)$ as the scale of $\rho_{1/2}$. It reduces equations (A 11) to

$$\left.\begin{aligned}\dot{\rho}_+ &= -\rho_+ + \rho_1\rho_2\cos\Theta\,,\\ \dot{\rho}_1 &= \mu\rho_1 + \rho_+\rho_2\cos(\Theta-\varphi)\,,\\ \dot{\rho}_2 &= \mu\rho_2 + \rho_+\rho_1\cos(\Theta+\varphi)\,,\\ \text{and}\qquad \dot{\Theta} &= -\frac{\rho_1\rho_2}{\rho_+}\sin\Theta - \rho_+\left(\frac{\rho_1}{\rho_2}\sin(\Theta+\varphi)+\frac{\rho_2}{\rho_1}\sin(\Theta-\varphi)\right),\end{aligned}\right\} \tag{A 12}$$

where $\mu = \mu_o k_o^2/(|\mu_+|k_+^2)$ and $\varphi$ are the two remaining free parameters.

## (b) Stationary solutions

Setting the time derivatives to zero defines stationary solutions. The first three equations of (A 12) give the stationary values of the amplitudes:

$$\rho_+ = \frac{|\mu|}{[\cos(\Theta-\varphi)\cos(\Theta+\varphi)]^{1/2}} \quad\text{and}\quad \rho_{1,2} = \left[-\frac{\mu}{\cos(\Theta\pm\varphi)\cos\Theta}\right]^{1/2}. \tag{A 13}$$

All amplitudes need to be positive, and hence, it follows from (A 13) that $\cos(\Theta\pm\varphi)<0$, i.e. $\pi/2<|\varphi|<\pi$. Using (A 13) in the equation for $\Theta$ in (A 12) defines the stationary values of $\Theta$ by

$$-\tan\Theta + \mu[\tan(\Theta-\varphi)+\tan(\Theta+\varphi)] = 0. \tag{A 14}$$

The trivial solution of (A 14) is $\Theta=0$, which is the symmetric stationary solution, since it follows from equations (A 13) that $\rho_+ = \rho_1^2 = \rho_2^2 = |\mu/\cos\varphi|$, i.e. left and right-travelling wave modes have the same amplitude. Non-zero $\Theta$ corresponds to asymmetric solutions. We use the identity

$$\begin{aligned}\tan(\Theta-\varphi)+\tan(\Theta+\varphi) &= \frac{\sin\Theta\cos\varphi-\cos\Theta\sin\varphi}{\cos\Theta\cos\varphi+\sin\Theta\sin\varphi}+\frac{\cos\Theta\sin\varphi+\sin\Theta\cos\varphi}{\cos\Theta\cos\varphi-\sin\Theta\sin\varphi}\\ &= \frac{2\cos\Theta\sin\Theta}{\cos^2\Theta\cos^2\varphi-\sin^2\Theta\sin^2\varphi}\end{aligned} \tag{A 15}$$

and transform (A 14) into

$$\left.\begin{aligned}-\tan\Theta+\mu\frac{2\cos\Theta\sin\Theta}{\cos^2\Theta\cos^2\varphi-\sin^2\Theta\sin^2\varphi} &= 0\\ \Rightarrow(1-\cos^2\Theta)\sin^2\varphi-\cos^2\Theta\cos^2\varphi+2\mu\cos^2\Theta &= 0\\ \Rightarrow(1-2\mu)\cos^2\Theta &= \sin^2\varphi.\end{aligned}\right\} \tag{A 16}$$

Since $(1-2\mu)\cos^2\Theta < 1-2\mu$, asymmetric solutions can only exist if $1-2\mu\geq\sin^2\varphi$, i.e. for $0\leq\mu\leq\frac{1}{2}\cos^2\varphi$. The acceptable interval of both angles, as well as the sign of $\mu$ would overturn if we had chosen $\mu_+>0$ in (A11).

## (c) Stability of stationary solutions

Next, we consider the stability of the symmetric and asymmetric solutions. For this, we determine the Jacobian matrix $\underline{\mathbf{J}}$,

$$\underline{\mathbf{J}} = \begin{pmatrix} -1 & \rho_2\cos\Theta & \rho_1\cos\Theta & -\rho_1\rho_2\sin\Theta\\ \rho_2\cos(\Theta-\varphi) & \mu & \rho_+\cos(\Theta-\varphi) & -\rho_+\rho_2\sin(\Theta-\varphi)\\ \rho_1\cos(\Theta+\varphi) & \rho_+\cos(\Theta-\varphi) & \mu & -\rho_+\rho_1\sin(\Theta-\varphi)\\ \dfrac{P-Q-R}{\rho_+^2\rho_1\rho_2} & \dfrac{-P+Q-R}{\rho_+\rho_1^2\rho_2} & \dfrac{-P-Q+R}{\rho_+\rho_1\rho_2^2} & -\dfrac{S}{\rho_+\rho_1\rho_2}\end{pmatrix} \tag{A 17}$$

with abbreviations

$$\left.\begin{aligned} &P=\rho_1^2\rho_2^2\sin\Theta\,, \quad Q=\rho_+^2\rho_2^2\sin(\Theta-\varphi)\,, \quad R=\rho_+^2\rho_1^2\sin(\Theta+\varphi)\\ \text{and}\qquad &S=\rho_1^2\rho_2^2\cos\Theta+\rho_+^2\rho_2^2\cos(\Theta-\varphi)+\rho_+^2\rho_1^2\cos(\Theta+\varphi)\end{aligned}\right\}. \tag{A 18}$$

Introducing the stationary solution into (A17), we compute the characteristic polynomial

$$\det(\lambda\underline{\mathbf{1}}-\underline{\mathbf{J}})=a_0\lambda^4+a_1\lambda^3+a_2\lambda^2+a_3\lambda+a_4=0 \tag{A 19}$$

with constant real coefficients $a_i$. We apply the Hurwitz criterion to analyse linear stability. For linear stability, the following conditions have to be fulfilled

$$a_1>0,\quad a_4>0,\quad a_1a_2-a_0a_3>0\quad\text{and}\quad (a_1a_2-a_0a_3)a_3-a_1^2a_4>0. \tag{A 20}$$

In particular, zero crossings of $a_4$ that is the determinant of $\underline{\mathbf{J}}$ indicate monotonic instabilities.

For the symmetric solution, the Jacobian matrix is

$$\underline{\mathbf{J}}_{\text{sym}}=\begin{pmatrix} -1 & \sqrt{\frac{-\mu}{\cos\varphi}} & \sqrt{\frac{-\mu}{\cos\varphi}} & 0\\ \sqrt{\frac{-\mu}{\cos\varphi}} & \mu & -\mu & \left(\frac{-\mu}{\cos\varphi}\right)^{3/2}\sin\varphi\\ \sqrt{\frac{-\mu}{\cos\varphi}} & -\mu & \mu & -\left(\frac{-\mu}{\cos\varphi}\right)^{3/2}\sin\varphi\\ 0 & -2\sqrt{\frac{-\mu}{\cos\varphi}}\sin\varphi & 2\sqrt{\frac{-\mu}{\cos\varphi}}\sin\varphi & -1+2\mu \end{pmatrix}, \tag{A 21}$$

and the Hurwitz criterion yields

$$2-4\mu>0, \tag{A 22}$$

$$4\mu^2(-1+2\mu+2\mu\tan^2\varphi)>0, \tag{A 23}$$

$$2-12\mu+28\mu^2-16\mu^3-4\mu^2(-1+4\mu)\tan^2\varphi>0 \tag{A 24}$$

$$\text{and}\qquad -4\mu^2(-1+4\mu)\left(1-3\mu+4\mu^2+(1-2\mu)\cos(2\varphi)+\mu\cos(4\varphi)\right)\sec^4\varphi>0. \tag{A 25}$$

In the following, we always consider the region $0\le\mu\le 1/2$, $\pi/2\le\varphi\le\pi$. Note that all results are invariant when $\varphi\to-\varphi$. Equation (A 22) holds for the considered parameter region. The other three conditions are plotted in figure 5, where the yellow regions in (*a*)–(*c*) correspond to positive values of the expression in equations (A 23)–(A 25), respectively. Together they yield $[\frac{1}{2}\cos^2\varphi, \frac{1}{4}]$ as the region of linear stability for the symmetric solution. At $\mu=\frac{1}{2}\cos^2\varphi$, where $a_4$ crosses zero, the asymmetric solution emerges from the symmetric one in a pitchfork bifurcation, and the latter is unstable for smaller $\mu$ values. At $\mu=\frac{1}{4}$ a Hopf bifurcation renders the symmetric solution unstable for larger $\mu$ values. At $\varphi=\frac{3}{4}\pi$, i.e. when $\frac{1}{2}\cos^2(\frac{3}{4}\pi)=\frac{1}{4}$ the pitchfork and the Hopf bifurcation merge at the double zero singularity and no stable symmetric solutions exist for $\varphi\ge\frac{3}{4}\pi$. For the asymmetric solution, the calculation is more involved since we must use some trigonometric relations to replace all $\Theta$ dependencies. First, from (A 14), we know

$$\tan(\Theta-\varphi)+\tan(\Theta+\varphi)=\frac{\tan\Theta}{\mu} \tag{A 26}$$

and

$$\tan^2(\Theta-\varphi)+\tan^2(\Theta+\varphi)=\frac{\tan^2\Theta}{\mu^2}-2\tan(\Theta-\varphi)\tan(\Theta+\varphi). \tag{A 27}$$

Furthermore,

$$\begin{aligned}\tan(\Theta-\varphi)+\tan(\Theta+\varphi)&=\frac{2\cos\Theta\sin\Theta}{\cos(\Theta+\varphi)\cos(\Theta-\varphi)}\\ &=\frac{2\tan\Theta}{(1+\tan^2\Theta)\cos(\Theta+\varphi)\cos(\Theta-\varphi)},\end{aligned}$$

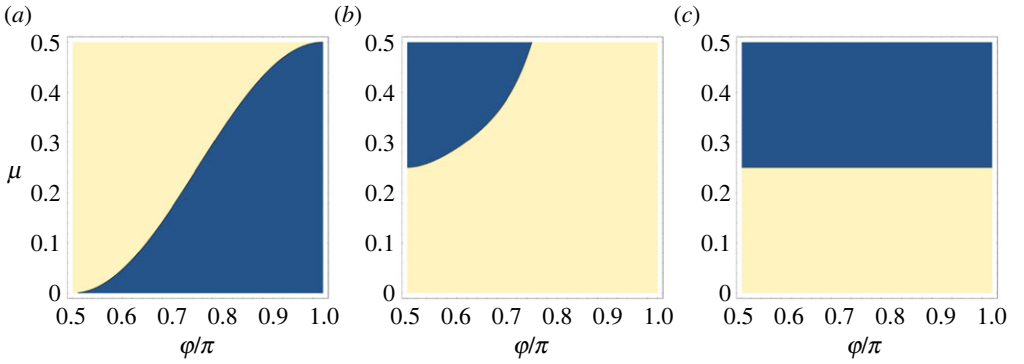


**Figure 5.** Hurwitz criterion for the symmetric solution, equations (*a*) (A 23), (*b*) (A 24) and (*c*) (A 25). Yellow (blue) regions correspond to positive (negative) values. (Online version in colour.)

and comparing with (A 26), it follows

$$\cos(\Theta+\varphi)\cos(\Theta-\varphi)=\frac{2\mu}{1+\tan^2\Theta}, \tag{A 28}$$

which can then be used to obtain

$$\begin{aligned}\tan^2(\Theta-\varphi)+\tan^2(\Theta+\varphi)&=\frac{\sin^2(2\Theta)+\sin^2(2\varphi)}{2\cos^2(\Theta+\varphi)\cos^2(\Theta-\varphi)}\\&=\frac{(\sin^2(2\Theta)+\sin^2(2\varphi))(1+\tan^2\Theta)^2}{8\mu^2}.\end{aligned} \tag{A 29}$$

Now, by inserting (A 29) into (A 27), we see that

$$16\mu^2\tan(\Theta-\varphi)\tan(\Theta+\varphi)=8\tan^2\Theta-(\sin^2(2\Theta)+\sin^2(2\varphi))(1+\tan^2\Theta)^2. \tag{A 30}$$

From (A 16), it follows that

$$\sin^2(2\varphi)=4\sin^2\varphi\cos^2\varphi=4(1-2\mu)\cos^2\Theta(1-(1-2\mu)\cos^2\Theta)$$

and

$$\sin^2(2\Theta)=4\cos^2\Theta\sin^2\Theta=4\cos^2\Theta(1-\cos^2\Theta),$$

which we insert into (A 30) and obtain

$$\tan(\Theta-\varphi)\tan(\Theta+\varphi)=\frac{-1+2\mu+\tan^2\Theta}{2\mu}. \tag{A 31}$$

Finally, by using (A 27), we can replace any $\tan^2\Theta$ via

$$\tan^2\Theta=\frac{1-(\sin^2\varphi/(1-2\mu))}{\sin^2\varphi/(1-2\mu)}=\frac{1-2\mu}{\sin^2\varphi}-1. \tag{A 32}$$

Next, by using the replacements (A 26), (A 27), (A 31) and finally (A 32), all coefficients of the Hurwitz criterion (A 20) are written as functions depending solely on $\mu$ and $\varphi$:

$$2(1-2\mu)>0, \tag{A 33}$$

$$4(1-2\mu)\mu(-1+(1-2\mu)\csc^2\varphi)>0, \tag{A 34}$$

$$\csc^2\varphi(5-28\mu+40\mu^2-16\mu^3-(-3+2\mu+4\mu^2)\cos(2\varphi))>0 \tag{A 35}$$

and

$$-4\mu\Big((4\mu-1)(1-5\mu+8\mu^2)+(3-16\mu+40\mu^2-16\mu^3)(-1+(1-2\mu)\csc^2\varphi)$$
$$+3(4-7\mu+4\mu^2)(-1+(1-2\mu)\csc^2\varphi)^2\Big)>0. \tag{A 36}$$

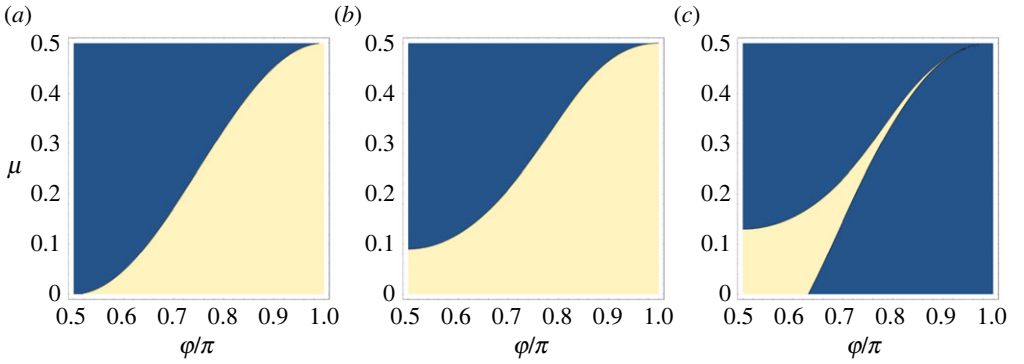


**Figure 6.** Hurwitz criterion for the asymmetric solution, equations (*a*) (A 34), (*b*) (A 35) and (*c*) (A 36). Yellow (blue) regions correspond to positive (negative) values. (Online version in colour.)

Equation (A 33) is always fulfilled for the considered $\mu$ values, and figure 6 illustrates equations (A 34)–(A 36) in (*a*)–(*c*), respectively. We see that figure 6*a* gives the pitchfork bifurcation to the symmetric stationary state and figure 6*b* does not apply taking into account the existence interval $0 \leq \mu \leq \frac{1}{2}\cos^2\varphi$. That is, figure 6*c* gives the lower stability border of the asymmetric solution. Rewriting the corresponding equation (A 36), we conclude that the asymmetric stationary state is stable if

$$-(4\mu-1)(1-5\mu+8\mu^2)\sin^4\varphi - 3(4-7\mu+4\mu^2)(\cos^2\varphi-2\mu)^2 - \Big(3+8\mu(\mu-2)(1-2\mu)\Big)(\cos^2\varphi-2\mu)\sin^2\varphi > 0. \tag{A 37}$$

The zero crossing of the left-hand side indicates the locus of the secondary Hopf bifurcation, which renders the asymmetric state unstable.

## References


1. Bowick MJ, Fakhri N, Marchetti MC, Ramaswamy S. 2022 Symmetry, thermodynamics, and topology in active matter. *Phys. Rev. X* **12**, 010501. (doi:10.1103/PhysRevX.12.010501)
2. Fruchart M, Hanai R, Littlewood PB, Vitelli V. 2021 Non-reciprocal phase transitions. *Nature* **592**, 363–369. (doi:10.1038/s41586-021-03375-9)
3. Kryuchkov NP, Mistryukova LA, Sapelkin AV, Yurchenko SO. 2020 Strange attractors induced by melting in systems with nonreciprocal effective interactions. *Phys. Rev. E* **101**, 063205. (doi:10.1103/PhysRevE.101.063205)
4. Popescu MN. 2020 Chemically active particles: from one to few on the way to many. *Langmuir* **36**, 6861–6870. (doi:10.1021/acs.langmuir.9b03973)
5. You ZH, Baskaran A, Marchetti MC. 2020 Nonreciprocity as a generic route to traveling states. *Proc. Natl Acad. Sci. USA* **117**, 19 767–19 772. (doi:10.1073/pnas.2010318117)
6. Chen YX, Kolokolnikov T. 2014 A minimal model of predator-swarm interactions. *J. R. Soc. Interface* **11**, 20131208. (doi:10.1098/rsif.2013.1208)
7. Frohoff-Hülsmann T, Wrembel J, Thiele U. 2021 Suppression of coarsening and emergence of oscillatory behavior in a Cahn-Hilliard model with nonvariational coupling. *Phys. Rev. E* **103**, 042602. (doi:10.1103/PhysRevE.103.042602)
8. Saha S, Agudo-Canalejo J, Golestanian R. 2020 Scalar active mixtures: the non-reciprocal Cahn-Hilliard model. *Phys. Rev. X* **10**, 041009. (doi:10.1103/PhysRevX.10.041009)
9. Frohoff-Hülsmann T, Holl MP, Knobloch E, Gurevich SV, Thiele U. 2022 Stationary broken parity states in nonvariational models. arXiv:2205.14364.
10. Schüler D, Alonso S, Torcini A, Bär M. 2014 Spatio-temporal dynamics induced by competing instabilities in two asymmetrically coupled nonlinear evolution equations. *Chaos* **24**, 043142. (doi:10.1063/1.4905017)

11. Matthews PC, Cox SM. 2000 Pattern formation with a conservation law. *Nonlinearity* **13**, 1293–1320. (doi:10.1088/0951-7715/13/4/317)
12. Winterbottom DM, Matthews PC, Cox SM. 2005 Oscillatory pattern formation with a conserved quantity. *Nonlinearity* **18**, 1031–1056. (doi:10.1088/0951-7715/18/3/006)
13. Knobloch E. 2016 Localized structures and front propagation in systems with a conservation law. *IMA J. Appl. Math.* **81**, 457–487. (doi:10.1093/imamat/hxw029)
14. Ophaus L, Gurevich SV, Thiele U. 2018 Resting and traveling localized states in an active phase-field-crystal model. *Phys. Rev. E* **98**, 022608. (doi:10.1103/PhysRevE.98.022608)
15. Thiele U, Archer AJ, Robbins MJ, Gomez H, Knobloch E. 2013 Localized states in the conserved Swift-Hohenberg equation with cubic nonlinearity. *Phys. Rev. E* **87**, 042915. (doi:10.1103/PhysRevE.87.042915)
16. Beta C, Gov NS, Yochelis A. 2020 Why a large-scale mode can be essential for understanding intracellular actin waves. *Cells* **9**, 1533. (doi:10.3390/cells9061533)
17. Yochelis A, Flemming S, Beta C. 2022 Versatile patterns in the actin cortex of motile cells: self-organized pulses can coexist with macropinocytic ring-shaped waves. *Phys. Rev. Lett.* **129**, 088101. (doi:10.1103/PhysRevLett.129.088101)
18. Cahn JW. 1965 Phase separation by spinodal decomposition in isotropic systems. *J. Chem. Phys.* **42**, 93–99. (doi:10.1063/1.1695731)
19. Cahn JW, Hilliard JE. 1958 Free energy of a nonuniform system. 1. Interfacial free energy. *J. Chem. Phys.* **28**, 258–267. (doi:10.1063/1.1744102)
20. Bergmann F, Rapp L, Zimmermann W. 2018 Active phase separation: a universal approach. *Phys. Rev. E* **98**, 020603. (doi:10.1103/PhysRevE.98.020603)
21. Bernitt E, Dobereiner HG, Gov NS, Yochelis A. 2017 Fronts and waves of actin polymerization in a bistability-based mechanism of circular dorsal ruffles. *Nat. Commun.* **8**, 15863. (doi:10.1038/ncomms15863)
22. Halatek J, Frey E. 2018 Rethinking pattern formation in reaction-diffusion systems. *Nat. Phys.* **14**, 507–514. (doi:10.1038/s41567-017-0040-5)
23. Ishihara S, Otsuji M, Mochizuki A. 2007 Transient and steady state of mass-conserved reaction-diffusion systems. *Phys. Rev. E* **75**, 015203. (doi:10.1103/PhysRevE.75.015203)
24. John K, Bär M. 2005 Alternative mechanisms of structuring biomembranes: self-assembly versus self-organization. *Phys. Rev. Lett.* **95**, 198101. (doi:10.1103/PhysRevLett.95.198101)
25. Tero A, Kobayashi R, Nakagaki T. 2005 A coupled-oscillator model with a conservation law for the rhythmic amoeboid movements of plasmodial slime molds. *Physica D* **205**, 125–135. (doi:10.1016/j.physd.2005.01.010)
26. Wettmann L, Bonny M, Kruse K. 2014 Effects of molecular noise on bistable protein distributions in rod-shaped bacteria. *Interface Focus* **4**, 20140039. (doi:10.1098/rsfs.2014.0039)
27. Fang X, Kruse K, Lu T, Wang J. 2019 Nonequilibrium physics in biology. *Rev. Mod. Phys.* **91**, 045004. (doi:10.1103/RevModPhys.91.045004)
28. Halatek J, Brauns F, Frey E. 2018 Self-organization principles of intracellular pattern formation. *Phil. Trans. R. Soc. B* **373**, 20170107. (doi:10.1098/rstb.2017.0107)
29. John K, Bär M. 2005 Travelling lipid domains in a dynamic model for protein-induced pattern formation in biomembranes. *Phys. Biol.* **2**, 123–132. (doi:10.1088/1478-3975/2/2/005)
30. Kreienkamp KL, Klapp SHL. 2022 Clustering and flocking of repulsive chiral active particles with non-reciprocal couplings. *New J. Phys.* **24**, 123009. (doi:10.1088/1367-2630/ac9cc3)
31. Kruse K, Joanny JF, Jülicher F, Prost J, Sekimoto K. 2005 Generic theory of active polar gels: a paradigm for cytoskeletal dynamics. *Eur. Phys. J. E* **16**, 5–16. (doi:10.1140/epje/e2005-00002-5)
32. Marchetti MC, Joanny JF, Ramaswamy S, Liverpool TB, Prost J, Rao M, Simha RA. 2013 Hydrodynamics of soft active matter. *Rev. Mod. Phys.* **85**, 1143–1189. (doi:10.1103/RevModPhys.85.1143)
33. Radszuweit M, Alonso S, Engel H, Bär M. 2013 Intracellular mechanochemical waves in an active poroelastic model. *Phys. Rev. Lett.* **110**, 138102. (doi:10.1103/PhysRevLett.110.138102)
34. Seirin-Lee S, Sukekawa T, Nakahara T, Ishii H, Ei SI. 2020 Transitions to slow or fast diffusions provide a general property for in-phase or anti-phase polarity in a cell. *J. Math. Biol.* **80**, 1885–1917. (doi:10.1007/s00285-020-01484-z)
35. Frohoff-Hülsmann T, Thiele U. 2023 Nonreciprocal Cahn-Hilliard equations emerging as one of eight universal amplitude equations. arXiv:2301.05568.

36. Frohoff-Hülsmann T, Thiele U. 2021 Localised states in coupled Cahn-Hilliard equations. *IMA J. Appl. Math.* **86**, 924–943. (doi:10.1093/imamat/hxab026)
37. Liehr A 2013 *Dissipative solitons in reaction diffusion systems: mechanisms, dynamics, interaction*. Springer Series in Synergetics. Berlin, Heidelberg: Springer.
38. Nishiura Y, Teramoto T, Ueda KI. 2003 Dynamic transitions through scattors in dissipative systems. *Chaos* **13**, 962–972. (doi:10.1063/1.1592131)
39. Nishiura Y, Watanabe T. 2022 Traveling pulses with oscillatory tails, figure-eight-like stack of isolas, and in media. *Physica D* **440**, 133448. (doi:10.1016/j.physd.2022.133448)
40. Purwins HG, Bödeker HU, Amiranashvili S. 2010 Dissipative solitons. *Adv. Phys.* **59**, 485–701. (doi:10.1080/00018732.2010.498228)
41. Menzel AM, Löwen H. 2013 Traveling and resting crystals in active systems. *Phys. Rev. Lett.* **110**, 055702. (doi:10.1103/PhysRevLett.110.055702)
42. Ophaus L, Kirchner J, Gurevich SV, Thiele U. 2020 Phase-field-crystal description of active crystallites: elastic and inelastic collisions. *Chaos* **30**, 123149. (doi:10.1063/5.0019426)
43. te Vrugt M, Holl MP, Koch A, Wittkowski R, Thiele U. 2022 Derivation and analysis of a phase field crystal model for a mixture of active and passive particles. *Model. Simul. Mater. Sci. Eng.* **30**, 084001. (doi:10.1088/1361-651X/ac856a)
44. Langer JS. 1992 An introduction to the kinetics of first-order phase transitions. In *Solids far from equilibrium* (ed. C Godrèche), pp. 297–363, Cambridge: Cambridge University Press.
45. Turing AM. 1952 The chemical basis of morphogenesis. *Phil. Trans. R. Soc. London B* **237**, 37–72. (doi:10.1098/rstb.1952.0012)
46. Holl MP, Archer AJ, Gurevich SV, Knobloch E, Ophaus L, Thiele U. 2021 Localized states in passive and active phase-field-crystal models. *IMA J. Appl. Math.* **86**, 896–923. (doi:10.1093/imamat/hxab025)
47. Tseluiko D, Alesemi M, Lin T-S, Thiele U. 2020 Effect of driving on coarsening dynamics in phase-separating systems. *Nonlinearity* **33**, 4449–4483. (doi:10.1088/1361-6544/ab8bb0)
48. Watson SJ, Otto F, Rubinstein BY, Davis SH. 2003 Coarsening dynamics of the convective Cahn-Hilliard equation. *Physica D* **178**, 127–148. (doi:10.1016/S0167-2789(03)00048-4)
49. Rapp L, Bergmann F, Zimmermann W. 2019 Systematic extension of the Cahn-Hilliard model for motility-induced phase separation. *Eur. Phys. J. E* **42**, 57. (doi:10.1140/epje/i2019-11825-8)
50. Speck T, Bialke J, Menzel AM, Löwen H. 2014 Effective Cahn-Hilliard equation for the phase separation of active Brownian particles. *Phys. Rev. Lett.* **111**, 218304. (doi:10.1103/PhysRevLett.112.218304)
51. Eyre DJ. 1993 Systems of Cahn-Hilliard equations. *SIAM J. Appl. Math.* **53**, 1686–1712. (doi:10.1137/0153078)
52. Ma YQ. 2000 Phase separation in ternary mixtures. *J. Phys. Soc. Jpn.* **69**, 3597–3601. (doi:10.1143/JPSJ.69.3597)
53. Mao S, Kuldinow D, Haataja MP, Košmrlj A. 2019 Phase behavior and morphology of multicomponent liquid mixtures. *Soft Matter* **15**, 1297–1311. (doi:10.1039/C8SM02045K)
54. Nauman EB, He DQ. 2001 Nonlinear diffusion and phase separation. *Chem. Eng. Sci.* **56**, 1999–2018. (doi:10.1016/S0009-2509(01)00005-7)
55. Li YI, Cates ME. 2020 Non-equilibrium phase separation with reactions: a canonical model and its behaviour. *J. Stat. Mech.* **2020**, 053206. (doi:10.1088/1742-5468/ab7e2d)
56. Okuzono T, Ohta T. 2003 Traveling waves in phase-separating reactive mixtures. *Phys. Rev. E* **67**, 056211. (doi:10.1103/PhysRevE.67.056211)
57. Zwicker D, Hyman AA, Jülicher F. 2015 Suppression of Ostwald ripening in active emulsions. *Phys. Rev. E* **92**, 012317. (doi:10.1103/PhysRevE.92.012317)
58. Pismen LM 2006 *Patterns and interfaces in dissipative dynamics*. Springer Series in Synergetics. Berlin, Heidelberg: Springer-Verlag.
59. Proctor MRE. 2001 Finite amplitude behaviour of the Matthews–Cox instability. *Phys. Lett. A* **292**, 181–187. (doi:10.1016/S0375-9601(01)00793-9)
60. Cross MC, Hohenberg PC. 1993 Pattern formation out of equilibrium. *Rev. Mod. Phys.* **65**, 851–1112. (doi:10.1103/RevModPhys.65.851)
61. Golovin AA, Nepomnyashchy AA, Pismen LM. 1994 Interaction between short-scale Marangoni convection and long-scale deformational instability. *Phys. Fluids* **6**, 34–48. (doi:10.1063/1.868090)

62. Pismen LM, Rubinstein BY. 1999 Quasicrystalline and dynamic planforms in nonlinear optics. *Chaos Solitons Fractals* **10**, 761–776. (doi:10.1016/S0960-0779(98)00026-5)
63. Yang LF, Dolnik M, Zhabotinsky AM, Epstein IR. 2002 Pattern formation arising from interactions between Turing and wave instabilities. *J. Chem. Phys.* **117**, 7259–7265. (doi:10.1063/1.1507110)
64. De Wit A. 1999 Spatial patterns and spatiotemporal dynamics in chemical systems. *Adv. Chem. Phys.* **109**, 435–513. (doi:10.1002/9780470141687.ch5)
65. DeWit A, Lima D, Dewel G, Borckmans P. 1996 Spatiotemporal dynamics near a codimension-two point. *Phys. Rev. E* **54**, 261–271. (doi:10.1103/PhysRevE.54.261)
66. Yang L, Dolnik M, Zhabotinsky AM, Epstein IR. 2002 Spatial resonances and superposition patterns in a reaction-diffusion model with interacting Turing modes. *Phys. Rev. Lett.* **88**, 208303. (doi:10.1103/PhysRevLett.88.208303)
67. Krischer K, Mikhailov A. 1994 Bifurcation to traveling spots in reaction-diffusion systems. *Phys. Rev. Lett.* **73**, 3165–3168. (doi:10.1103/PhysRevLett.73.3165)
68. Fauve S, Douady S, Thual O. 1991 Drift instabilities of cellular-patterns. *J. Phys. II* **1**, 311–322. (doi:10.1051/jp2:1991170)
69. Frohoff-Hülsmann T, Thiele U, Pismen LM. 2023 Non-reciprocity induces resonances in a two-field Cahn–Hilliard model. Zenodo. (doi:10.5281/zenodo.7503482)